



DEGREE PROJECT IN SYSTEMS ENGINEERING,  
SECOND CYCLE, 30 CREDITS  
*STOCKHOLM, SWEDEN 2024*

# **Modelling of control systems for flight of wing in ground effect craft**

Marcus Mhanna

**Author**

Marcus Mhanna <[mmhanna@kth.se](mailto:mmhanna@kth.se)>  
Master's Programme, Aerospace Engineering, 120 credits  
KTH Royal Institute of Technology

**Supervisor**

Associate Prof. Raffaeallo Mariani <[rmariani@kth.se](mailto:rmariani@kth.se)>  
Department of Engineering Mechanics  
KTH Royal Institute of Technology

**Examiner**

Associate Prof. Per Enqvist <[penqvist@kth.se](mailto:penqvist@kth.se)>  
Department of Mathematics  
KTH Royal Institute of Technology

**Place for Project**

Stockholm, Sweden

Date: October, 2024

---

# Contents

<b>1</b>	<b>Introduction</b>	<b>1</b>
1.1	Background . . . . .	1
1.2	Problem . . . . .	2
1.2.1	Original problem and definition . . . . .	2
1.2.2	Scientific and engineering issues . . . . .	2
1.3	Objectives and Goals . . . . .	3
1.3.1	Goals . . . . .	3
1.4	Research Methodology . . . . .	3
1.5	Delimitations . . . . .	4
1.6	Structure of the thesis . . . . .	4
<b>2</b>	<b>Analysis and Literature study</b>	<b>5</b>
2.1	Aerodynamic Forces Estimation . . . . .	5
2.1.1	Prandtl Lifting-Line Wing Theory . . . . .	5
2.1.2	Equations of Motion . . . . .	7
2.1.3	Ground effect . . . . .	9
2.1.4	Vortex Lattice Method . . . . .	12
2.2	Longitudinal Control System . . . . .	13
2.2.1	Initial Control Analysis . . . . .	13
2.2.2	Pairing Problem and Decentralized Control . . . . .	15
2.2.3	H-infinite Robust Control . . . . .	16
2.2.4	Infinite time Optimal Control . . . . .	18
<b>3</b>	<b>Methodology</b>	<b>21</b>
3.1	Research Process and Gathering Data . . . . .	21
3.1.1	Aerodynamics: Lifting Line Method . . . . .	21
3.1.2	Aerodynamics: Vortex Lattice . . . . .	26
3.2	Flight Simulator and Open Loop System . . . . .	27
3.2.1	Flight Simulator . . . . .	27
3.3	Control Design Methods . . . . .	28
3.3.1	Pairing Problem and Decentralized Controller . . . . .	28
3.3.2	Robust $H_\infty$ Controller . . . . .	29
3.3.3	Optimal Controller . . . . .	30
<b>4</b>	<b>Results and Analysis</b>	<b>33</b>

4.1	Modeled Aerodynamics . . . . .	33
4.1.1	Lift Coefficient Elevator Setting . . . . .	33
4.1.2	Lift to Drag Ratio . . . . .	34
4.1.3	Performance Analysis . . . . .	34
4.2	Modelling of Dynamics and Open Loop System . . . . .	37
4.2.1	Open Loop System . . . . .	37
4.3	Control Systems . . . . .	39
4.3.1	Pairing Problem and Decentralized Controller . . . . .	39
4.3.2	H-infinite Controller . . . . .	40
4.3.3	Optimal Quadratic Controller . . . . .	41
4.3.4	Performance Control Analysis . . . . .	43
4.3.5	Stability Analysis . . . . .	44
<b>5</b>	<b>Discussion</b>	<b>47</b>
5.0.1	Generated Aerodynamics . . . . .	47
5.0.2	Implemented Control Systems . . . . .	47
<b>6</b>	<b>Conclusions and Future work</b>	<b>49</b>
6.1	Conclusions . . . . .	49
6.2	Limitations . . . . .	50
6.3	Future work . . . . .	50
6.3.1	What has been left undone? . . . . .	50
6.3.2	Next obvious things to be done . . . . .	50
6.4	Reflections . . . . .	50
	<b>References</b>	<b>51</b>

# Modelling of control systems for flight of wing in ground effect craft

MScAE Marcus Mhanna

December 23, 2024

## Abstract

The concerns for climate change is ever increasing and that led to a large movement to make the modes of transport in general more sustainable. However, with modern technology on batteries and electric engines, this could not be feasible, instead a look for more favourable environments to operate the modes of transport could be the solution here, and more specifically ground effect. The main focus of this thesis is to stabilize a craft in ground effect longitudinally in cruising mode. The craft will be flying at 0.5 m over a wavy surface where a lot of disturbances will occur and the margin for error is really small. The aerodynamics together with the ground effect model over a wavy surface are studied and the data is generated from models and simulations. Two methods are used for aerodynamics data generation, the first one is lifting line method and the second one is Vortex Lattice method, and they are compared and evaluated. The ground effect model is integrated into an aerodynamic model to check how it will affect the aerodynamics of the craft. These methods will be used as a test block for the control systems implementations. Two approaches to building the control algorithm are used which are  $H_\infty$  robust control and infinite time horizon optimal control. The two different approaches are implemented and compared at the end of the thesis with a discussion and evaluation on the performance of each one.

## Keywords

- Longitudinal Stability
- Ground effect
- Wavy Surface
- Robust Control
- Optimal Control



## Sammanfattning

Den ökande oron för klimatkrisen har gett upphov till en global rörelse för att elektrifiera alla flygresor runt världen. Eftersom den nuvarande teknik för batterier och elektriska motorer har begränsningar, kan det vara mer realistiskt att undersöka alternativa och mer anpassande tillämpningar, såsom markeffekt. Detta examensarbete fokuserar på att stabilisera farkosten i markeffekt longitudinellt i marschflygning. Farkosten ska flyga på en höjd av 0.5 m över en vågig yta med störningar. Aerodynamiken med markeffekt ska modelleras, och data ska samlas in från simuleringar. Två metoder används för att samla aerodynamiska data: lifting line metoden och vortex lattice metoden. Dessa metoder kommer att jämföras och utvärderas i slutet av arbetet. Markeffekt integreras i själva modellen för att analysera dess inverkan på farkostens aerodynamiska prestanda. Den insamlade datan används som grund för att utveckla och modellera ett reglersystem. Två reglerstrategier tillämpas och utvärderas: en robust  $H_\infty$  regulator och en optimal regulator för oändlig horisont. De två metoderna implementeras och jämförs utifrån deras prestanda.

## Nyckelord

- Longitudinell Stabilitet
- Markeffekt
- Vågig Yta
- Robust Reglerteori
- Optimal Reglerteori



## Acknowledgments

I would like to thank my supervisor Raffaello Mariani for his continuous support and guidance throughout the project. I would like to also thank my examiner Per Enqvist for his occasional feedback on the project progression and valuable insights on the different aspects of the thesis.

Stockholm, December 2024



# List of Figures

1.1	Wing in ground effect (WIG) inner structure [7] . . . . .	2
2.1	Illustration of the local lift, drag and effective angle of attack along the wing in coordinates $y$ [8] . . . . .	6
2.2	Wake sheet strength related to wing's spanwise circulation gradient[8]. . . . .	7
2.3	Comparison between Weiselberger and McCormick formulations . . . . .	10
2.4	Schematic of the classical vortex lattice method by [12]. . . . .	12
2.5	Typical decentralized decoupled two inputs two outputs closed loop [14] . . . . .	15
2.6	Modeled uncertainty in closed loop system.[13] . . . . .	16
2.7	Block diagram for the extended closed loop system [15] . . . . .	17
3.1	Workbench layout for the method . . . . .	21
3.2	Airfoil for the tail NACA0008 . . . . .	22
3.3	Airfoil for the wing K3311 . . . . .	22
3.4	3-view drawing [7] . . . . .	23
3.5	Influence on the aerodynamics forces . . . . .	23
3.6	A lifting surface moving in proximity to the wavy ground from Rozhdestvensky [18] . . . . .	24
3.7	Ground effect influence on the wing above surface . . . . .	25
3.8	The lift to drag ratio (Lift to Drag ratio (LD)) for Airfoil K3311 at Reynolds number = 350000. . . . .	25
3.9	The lift to drag ratio (LD) for Airfoil N0008 at Reynolds number = 350000. . . . .	25
3.10	3D plane view in XFlr . . . . .	26
4.1	The pitching moment and lift dependent on elevator set with Lifting Line Model (LLM) . . . . .	33
4.2	The pitching moment and lift dependent on elevator set with Vortex Lattice Method (VLM) . . . . .	33
4.3	Lift to drag ration using LLM . . . . .	34
4.4	Lift to drag ratio using VLM . . . . .	34
4.5	Drag coefficient dependent on angle of attack using LLM . . . . .	34
4.6	Drag coefficient dependent on angle of attack using VLM . . . . .	34
4.7	The trimmed vs untrimmed lift coefficient using LLM . . . . .	35
4.8	The trimmed vs untrimmed lift coefficient using VLM . . . . .	35
4.9	The lift data In Ground Effect (IGE) and Out Ground Effect (OGE) with LLM . . . . .	36
4.10	The lift data IGE and OGE with VLM . . . . .	36

4.11 Elevator trim angle over airspeed with LLM . . . . .	36
4.12 Elevator trim angle over airspeed with VLM . . . . .	36
4.13 Flight simulation for the vehicle in trim condition (cruise) . . . . .	37
4.14 Flight simulation for the vehicle with faulty inputs . . . . .	37
4.15 The Short period mode over airspeeds between [16-36] $m/s$ . . . . .	38
4.16 The Phugoid mode over airspeed between [16-36] $m/s$ . . . . .	38
4.17 The step response of the open loop system . . . . .	38
4.18 The impulse response of the open loop system . . . . .	38
4.19 System gain for the open loop system . . . . .	39
4.20 The step response of DC closed loop system . . . . .	40
4.21 The impulse response of DC closed loop System . . . . .	40
4.22 The step response of $H_\infty$ closed loop system . . . . .	40
4.23 The impulse response of $H_\infty$ closed loop System . . . . .	40
4.24 System gain for the $H_\infty$ controller . . . . .	41
4.25 The step response of the Open Loop System . . . . .	42
4.26 The Impulse response of the Open Loop System . . . . .	42
4.27 System gain for the LQ optimal controller . . . . .	43
4.28 System gain comparison between $LQ$ and $H_\infty$ . . . . .	44

# List of Tables

3.1	Preliminary data . . . . .	22
3.2	Ground Effect (GE) vehicle wing geometry . . . . .	26
4.1	Maximum lift to drag ratio . . . . .	35
4.2	Pairing problem solution . . . . .	39
4.3	Numerical results of the controllers performnace . . . . .	44



## List of acronyms and abbreviations

**ARE** Algebraic Riccati Equation

**CFD** Computational Fluid Dynamics

**EOM** Equations of Motion

**GE** Ground Effect

**HJBE** Hamiltonian Jacobi Bellman Equation

**IGE** In Ground Effect

**LD** Lift to Drag ratio

**LLM** Lifting Line Model

**MIMO** Multi Input Multi Output

**ODE** Ordinary Differential Equations

**OGE** Out Ground Effect

**RGA** Relative Gain Array

**SISO** Single Input Single Output

**SVD** Singular Value Decomposition

**VLM** Vortex Lattice Method

**WIG** Wing in ground effect



# Chapter 1

## Introduction

### 1.1 Background

The aviation industry accounts for a large part of the economics of the human life. The connectivity that the aviation industry provides for the economies help a lot in efficiently reducing time and cost for a lot of goods and transportation [1]. That helps to raise the standard of the living and makes these economies dependent on the aviation as an important part of the economic cycle. However, the aviation industry also accounts for 2.5 percent of the carbon footprint [2]. The latest studies proves that the the emissions that could harm the environment from the aviation is not limited to the carbon it produces but also other emissions (effective radiation). The real contribution of aviation according to the latest estimates are 4.5 percent [2]. With the new goals set from United Nations to cut down on carbon emissions, it sparked a movement to electrify aviation to make it greener and minimize emissions [3].

This is not an easy task given the current technology on electric propulsion where the range and power of the electric engines is not comparable to the commonly used combustion engine. The current electric aircraft models like the one from Heart Aerospace has a range of 400 km [4]. That means cross continent travel will not be possible, and some flight inside of Europe will require multiple stops to charge the aircraft. The advantage of traveling by aircraft which is mainly speed is going to be less, not to mention the strict safety rules which will make travels a lot more time consuming. The added mass of the batteries does also constraint the aircraft and affects its performance [5]. These questions are being researched and investigated in many campuses and institutions around the world where new models and optimization of aircraft designs are tested.

However, there is another possible solution that can be investigated which is trying to find a better and more favorable flying environment for the aircraft given our current technology. That environment is the ground effect. The ground effect is a phenomena that is well known and well studied in aviation. When the aircraft is close to the ground, the drag is reduced and lift is increased which means the aircraft is more efficient and requires less power from the engine to fly [6]. This will be further explained in the next chapter. Due to that fact the flying in ground effect means better efficiency, the common surface that is used for ground effect benefits are sea surfaces because it is the safer and landing on water is softer in case of emergency than landing on hard ground surface. The disadvantage with that choice is usually wavy nature that the sea surface have which causes the ground effect to change and that will produce disturbances in aerodynamics that has to be taken into account when

flying in these types of planes.

## 1.2 Problem

The project will focus on an existing electric vehicle in ground effect (an aircraft that fly in ground effect to minimize drag and maximize efficiency) project done in KTH. The main challenges are the generation of aerodynamic data for the vehicle in ground effect. The second problem is the longitudinal stability of the vehicle and finding methods and solutions to make it closed loop stable.

### 1.2.1 Original problem and definition

Using the existing wing in ground effect **WIG** design by a team from KTH light weight lab shown in Figure 1.1, a performance and aerodynamic analysis on the aircraft will be done. This performance and aerodynamic data is used in making a simulation for an open loop system where different maneuvers will be performed. Using the data and the dynamic system from the simulation, a closed feedback loop control system will be designed with different approaches and methods to meet different requirements such as optimality and robustness of the control system.

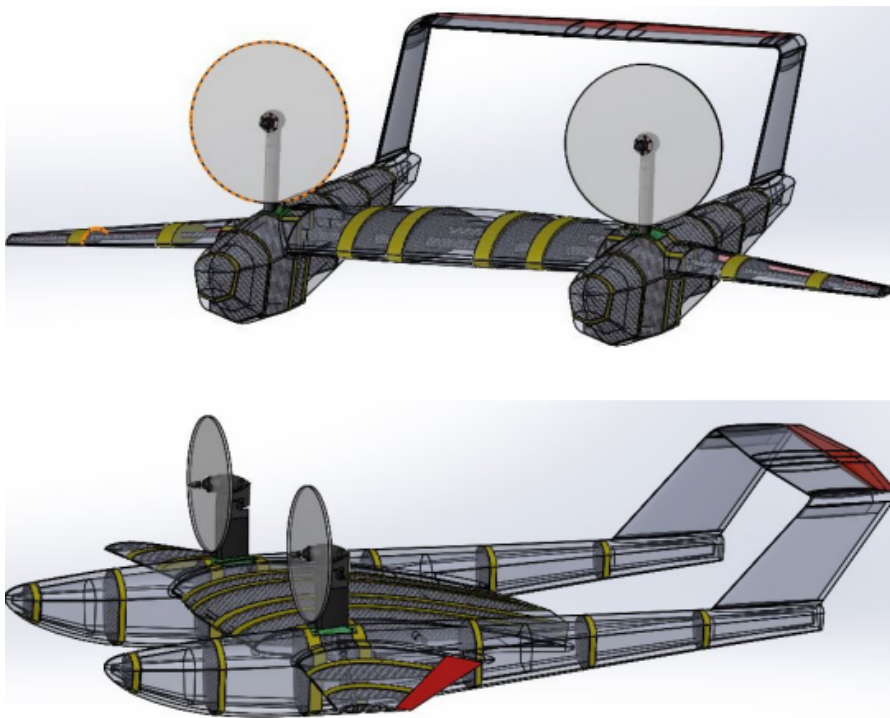


Figure 1.1: WIG inner structure [7]

### 1.2.2 Scientific and engineering issues

The project will focus on the modeling and simulation of the flight in ground effect. These simulations will be the base on which the different methods and approaches of control theory will be tested on. Therefore the first engineering challenge is that the testing on the vehicle itself will not be possible and for that the result of the control system has to be as robust as possible as the model can differ

from reality and that can make the results less meaningful. Another important aspect is that the vehicle aerodynamics model will use numerical methods and it will be compared to other data to check the logic behind it. Some safety margins like under estimations on the lift and over estimations on the drag will be implemented in the simulation to make sure the results will be useful even if the aerodynamics are not exactly accurate.

## 1.3 Objectives and Goals

The main objective is to analyze the open loop control system and develop multiple closed loop control approaches to test its efficiency and stability during flight as the flight height above the ground is relatively small (around 50-70 cm). The big picture will be to model and simulate the dynamic system and its aerodynamics and implementing an appropriate control system to use. The scientific purpose of the project is to study the different approaches possible to control the wing in ground effect in its relevant environment. The different control systems will be tested to see how they handle increase disturbance.

### 1.3.1 Goals

- (1) Model of the vehicle aerodynamics and ground effect.
- (2) Build a simple feedback loop control system and test the stability model.
- (3) Study the system gain of the closed loop and improve the control systems robustness by looking at different approaches and implementing model uncertainty.
- (4) Optimize the feedback control system by implementing Dynamic programming into the feedback loop to ensure optimal and efficient flight.

## 1.4 Research Methodology

The wing in ground effect design by KTH is going to be used as base for implementation, however the methods for control and approximating the ground effect will be independent of the aerodynamic data so that the analysis will be useful as a stepping stone for future project on flight by ground effect and implementation for control systems in ground effect. The control system implementation and the approaches that will be analyzed and studied are robust controls in model uncertainties so they can still be useful even if the aerodynamic model is not generating good approximations of the real aerodynamics. The focus on dividing the process into independent phases and parts is due to the lack of wind tunnel data which could be useful to verify that the Lifting Line Method **LLM** that will be used is not over estimating the aerodynamics of the craft. Instead an off the shelf software using Vortex Lattice Method **VLM** will be used to compare and validate with **LLM**. As it is highlighted in the Section 1.1, the big constraint in these types of designs are the battery and the range, and for that, optimal control will be also studied and compared to the robust approach, as it will be provide insight on the trade off between performance and robustness.

## 1.5 Delimitations

The project will not perform any extensive analysis on the ground effect and aerodynamics. The work will limit its aerodynamic data to the one from the LLM and VLM. Many sources would recommend that the ground effect is best analyzed using Computational Fluid Dynamics (CFD), but this will not be considered or studied as it is beyond the scope of the current work.

The control systems approaches are limited to two methods which are robust control and optimal control. The scope of this project will also consider the pairing problem from decentralized controller design for analysis but will not be the main focus of the project.

## 1.6 Structure of the thesis

Chapter 2 presents literature study and discusses and summarizes the theory on the subject. Chapter 3 explains the methods of how the problem is handled and how the different data will be determined to implement the control systems on. Chapter 4 showcases the obtained results using the aforementioned models and compares the results from the different methods. Chapter 5 presents explanations to model behavior and further performance analysis. Chapter 6 discusses future work and conclude the project and talks about the goals and objectives and their connection to the results with final notes.

# Chapter 2

## Analysis and Literature study

### 2.1 Aerodynamic Forces Estimation

#### 2.1.1 Prandtl Lifting-Line Wing Theory

To compute the aerodynamic forces estimation for the vehicle, a nonlinear lifting line model is considered. The lifting line model is heavily based on the Prandtl theory which has the advantage of being cheap to compute and provides simple and accurate results to build the flight simulation.

The lifting line analysis is in general based on the assumptions that each section of the wing acts as 2 dimensional airfoil with an effective angle of attack, and that the second one is the 2D airfoil flows have linear dependencies by neglecting viscosity effects [8]. The biggest advantage of the lifting line model is that it makes an effective use of the known 2D airfoil characteristics [8]. The near field flow is 2D with its lift  $L$  and drag  $D$  can be described as coefficients  $c_l$ ,  $c_d$  dependent on the section shape of the wing in that location [8] as described in the assumptions :

$$L'(y) = \frac{1}{2}\rho_{\infty}V_{\infty}^2c_{wing}c_l(\alpha_{eff}) \quad (2.1)$$

$$D'(y) = \frac{1}{2}\rho_{\infty}V_{\infty}^2c_{wing}c_d(\alpha_{eff}) \quad (2.2)$$

$$\alpha_{eff}(y) = \alpha + \alpha_{aero} - \alpha_i \quad (2.3)$$

There  $L'(y)$  and  $D'(y)$  are the sectioned lift and drag in location  $y$  along the wing. The value  $V_{\infty}$  is the free steam (wind) velocity [m/s],  $\rho_{\infty}$  is the air density, and  $c_{wing}$  is the wing chord. The angle  $\alpha_{eff}$  is the effective local angle of attack,  $\alpha_{aero}$  is the aerodynamic twist which is the local zero-lift line above the wing's reference axis, and  $\alpha_i$  is the induced angle of attack.

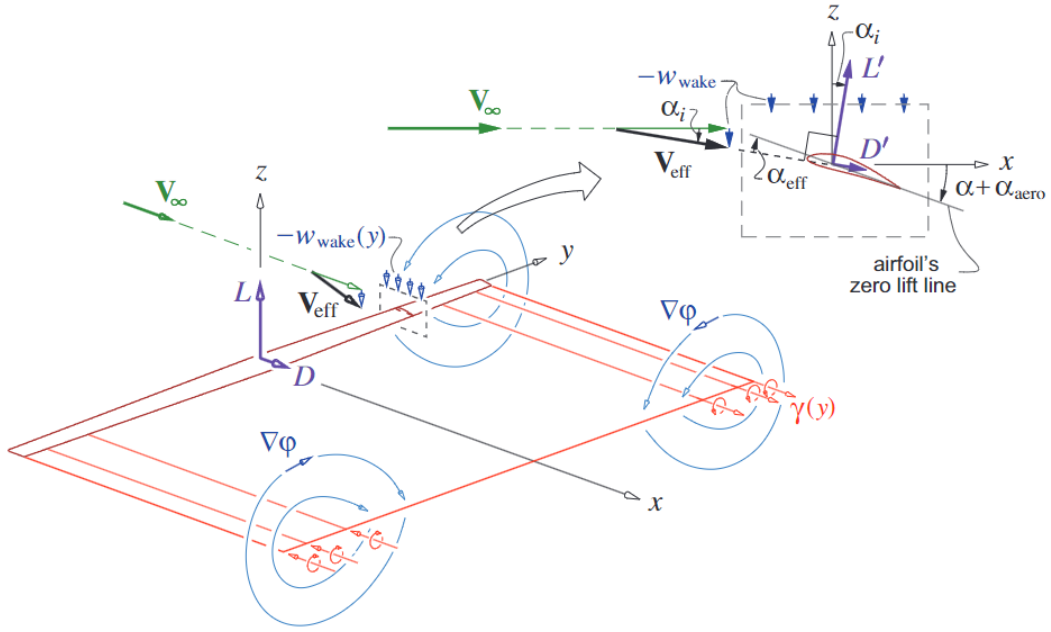


Figure 2.1: Illustration of the local lift, drag and effective angle of attack along the wing in coordinates  $y$  [8]

All parameters are shown on the 2D airfoil in the corner of the Figure 2.1. Now a projection of the sectioned lift and drag along the wing is needed to compute the global lift and drag over the whole wing by integrating over the span resulting in:

$$L = \int (L' \cos \alpha_i - D' \sin \alpha_i) dy \approx \int L' dy \quad (2.4)$$

$$D = \int (D' \cos \alpha_i + L' \sin \alpha_i) dy \approx D_p + D_i \quad (2.5)$$

$$D_p = \int D' dy \quad , \quad D_i = \int L' \alpha_i dy \quad (2.6)$$

There,  $D_p$  is the pressure drag and  $D_i$  is the induced drag. The division of the drag into two separate components is a result of lifting line force analysis [8]. The computation of the aerodynamic forces in Equations 2.4 and 2.5, requires the determination of the vortex sheet strength distribution  $\gamma(y)$  which can be related the wing circulation  $\Gamma(y)$  through the downwash velocity and the resulting induced angle in the following formula [8]:

$$w_{wake}(y) = \frac{1}{4\pi} \int_{-\frac{b}{2}}^{\frac{b}{2}} \frac{d\Gamma dy'}{dy'(y' - y)} \quad (2.7)$$

$$\alpha_i(y) = \frac{-w_{wake}}{V_\infty} \quad (2.8)$$

The relation between  $\Gamma$  and  $c_l$  in 2D airfoil is formulated as:

$$\Gamma = \frac{L'}{\rho V_\infty} = \frac{1}{2} V_\infty c c_\ell \quad (2.9)$$

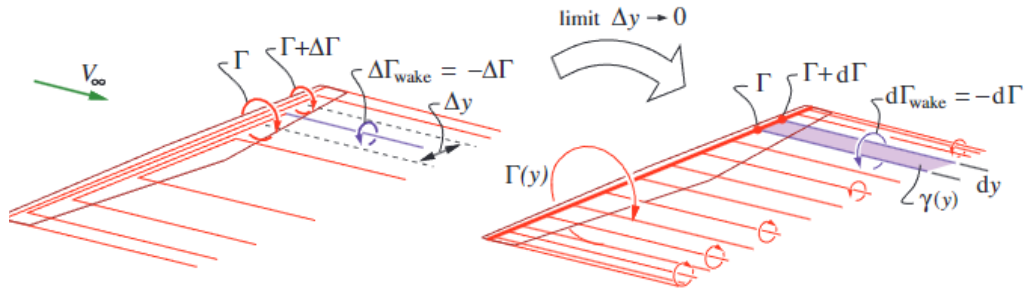


Figure 2.2: Wake sheet strength related to wing's spanwise circulation gradient[8].

leads to the relation between  $\Gamma$  and  $\alpha_i$ :

$$\Gamma = \frac{1}{2} V_{\infty} c_{l\alpha} c (\alpha + \alpha_{aero} - \alpha_i) \quad (2.10)$$

There,  $c_{l\alpha}$  is the lift slope curve which conveniently can be assumed to have linear dependence in 2D airfoil [8] and  $\alpha_{aero}$  is the aerodynamic twist as mentioned before, and both are calculated according to :

$$c_l = c_{l\alpha} (\alpha + \alpha_{aero} - \alpha_i) \quad (2.11)$$

$$\alpha_{aero}(y) = \alpha_{geom} - \alpha_{L=0} \quad (2.12)$$

Which includes both  $\alpha_{geom}$  the geometric twist and  $\alpha_{L=0}$  the zero lift angle. As shown in Equation (2.10),  $\Gamma$  depends on  $\alpha_i$  which is dependent on the overall  $\Gamma(y)$  and the superposition of  $w_{wake}$  calculated through Equation (2.7). To solve the unknown  $\Gamma(y)$ , a Fourier sine series is used in angle coordinates  $\vartheta = 0, 1 \dots \pi$ . A more extensive derivation of the method of how to formulate and solve  $\Gamma$  and  $w_{wake}$  with Fourier series can be found in Flight Vehicle Aerodynamics by Drela [8]. Now with the series terms of circulation and downwash :

$$\Gamma(\vartheta) = \Gamma(y(\vartheta)) = 2bV_{\infty} \sum_{n=1}^{\infty} \mathcal{A}_n \sin(n\vartheta) \quad (2.13)$$

$$w_{wake}(\vartheta) = -V_{\infty} \sum_{n=1}^{\infty} n \mathcal{A}_n \frac{\sin(n\vartheta)}{\sin(\vartheta)} \quad (2.14)$$

Combining (2.8), (2.11) and (2.10) and substituting with Fourier series (2.13) and (2.14), it results in the following algebraic relation between the coefficients  $\mathcal{A}_n$ :

$$\sum_{n=1}^{\infty} \mathcal{A}_n \left( \sin(n\vartheta) + \frac{c(\vartheta)}{4b} c_{l\alpha} n \frac{\sin(n\vartheta)}{\sin(\vartheta)} \right) = \frac{c(\vartheta)}{4b} c_{l\alpha} (\alpha - \alpha_{aero}(\vartheta)) \quad (2.15)$$

This method is mostly used for aerodynamics estimation of an aircraft. The inclusion of the ground effect contribution will be studied in Section 2.1.3.

## 2.1.2 Equations of Motion

One of the objectives of the project is to simulate the motion of the vehicle; therefore, the motion needs to be described through a mathematical formulation. The state vector is setup to show the

variables that will describe the movement of the vehicle.

$$x(t) = \left\{ \begin{array}{ccc} \underbrace{x^e \ y^e \ z^e}_{\text{Earth Axes}} & \underbrace{\phi \ \theta \ \psi}_{\text{Euler angle rates}} & \underbrace{u \ v \ w}_{\text{velocity}} \ \underbrace{p \ q \ r}_{\text{Angular Rotation}} \end{array} \right\} \quad (2.16)$$

For the control vector, it includes the variables that are used to change and affect the state of the system. These control variables are also called the input variables.

$$\delta(t) = \left\{ \delta_a \ \delta_e \ \delta_r \ \delta_f \ \delta_T \right\} \quad (2.17)$$

There, the first four variables represent the control surfaces of the aircraft, in order the  $\delta_a$  is the control input for the aileron,  $\delta_e$  is for the elevator,  $\delta_r$  is for the rudder,  $\delta_f$  is for the flaps, and  $\delta_T$  is for the throttle. With all the above variables in mind, the general equations of motion [8] can be formulated:

$$\begin{aligned} \dot{x}^e &= (\cos\theta \cos\psi)u + (\sin\phi \sin\theta \cos\psi - \cos\phi \sin\psi)v + (\cos\phi \sin\theta \cos\psi + \sin\phi \sin\psi)w \\ \dot{y}^e &= (\cos\theta \sin\psi)u + (\sin\phi \sin\theta \sin\psi + \cos\phi \cos\psi)v + (\cos\phi \sin\theta \sin\psi - \sin\phi \cos\psi)w \\ \dot{z}^e &= (-\sin\theta)u + (\sin\phi \cos\theta)v + (\cos\phi \cos\theta)w \\ \dot{\phi} &= p + q \sin\phi \tan\theta + r \cos\phi \tan\theta \\ \dot{\theta} &= q \cos\phi - r \sin\phi \\ \dot{\psi} &= q \sin\phi / \cos\theta + r \cos\phi / \cos\theta \\ X - mg \sin\theta &= m(\dot{u} + qw - rv) \\ Y + mg \sin\phi \cos\theta &= m(\dot{v} + ru - pw) \\ Z + mg \cos\phi \cos\theta &= m(\dot{w} + pv - qu) \\ \mathcal{L} &= I_{xx}\dot{p} + I_{xy}\dot{q} + I_{xz}\dot{r} + (I_{zz} - I_{yy})qr + I_{yz}(q^2 - r^2) + I_{xz}pq - I_{xy}pr + h_zq - h_yr \\ \mathcal{M} &= I_{xy}\dot{p} + I_{yy}\dot{q} + I_{yz}\dot{r} + (I_{xx} - I_{zz})rp + I_{xz}(r^2 - p^2) + I_{xy}qr - I_{yz}qp + h_xr - h_zp \\ \mathcal{N} &= I_{xz}\dot{p} + I_{yz}\dot{q} + I_{zz}\dot{r} + (I_{zz} - I_{xx})pq + I_{xy}(p^2 - q^2) + I_{yz}rp - I_{xz}rq + h_y p - h_x q \end{aligned} \quad (2.18)$$

There  $X, Y, Z$  are the aerodynamic forces and  $\mathcal{L}, \mathcal{M}, \mathcal{N}$  are the moments. Through reformulations of moments and aerodynamic forces, linear velocity rates  $[\dot{u}, \dot{v}, \dot{w}]$  and angular velocity rates  $[\dot{p}, \dot{q}, \dot{r}]$  can be derived. For the scope of this project, only longitudinal dynamics are studied. The variables considered are  $x_e$  and  $y_e$  representing the navigation variables in terms of distance and altitude,  $\dot{u}$  and  $\dot{w}$  representing the horizontal and vertical velocity rates, and finally  $\dot{\theta}$  and  $\dot{p}$  representing the pitch angle and the pitch rate angle. These equations must first be linearized, using the small perturbation theory [9].

### Linearization:

The method assumes that the steady condition is a reference and the motion of the vehicle is deviation from the said reference. In this case, the steady condition is a straight flight with zero heading rate. By implementing the small perturbations into the model and considering small disturbances  $\Delta$  as shown in the following model [8]:

$$\begin{aligned}
\mathbf{x}(t) &= \mathbf{x}_0 + \Delta\mathbf{x}(t) \\
\delta(t) &= \delta_0 + \Delta\delta(t) \\
\dot{\mathbf{x}}_0 + \Delta\dot{\mathbf{x}} &= \mathbf{f}(\mathbf{x}_0 + \Delta\mathbf{x}, \delta_0 + \Delta\delta) \simeq \mathbf{f}(\mathbf{x}_0, \delta_0) + \left. \frac{d\mathbf{f}}{d\mathbf{x}} \right|_{\mathbf{x}_0, \delta_0} \Delta\mathbf{x} + \left. \frac{d\mathbf{f}}{d\delta} \right|_{\mathbf{x}_0, \delta_0} \Delta\delta
\end{aligned} \tag{2.19}$$

An exponential growth in the disturbance can lead to big deviation from the reference condition which therefore can indicate instability. The linearization method leads to the following longitudinal dynamics system [8]:

$$\begin{pmatrix} \Delta\dot{u} \\ \Delta\dot{w} \\ \Delta\dot{q} \\ \Delta\dot{\theta} \end{pmatrix} = \begin{bmatrix} \frac{X_u}{m} & \frac{X_w}{m} & 0 & -g\cos\theta_0 \\ \frac{Z_u}{m-Z_{\dot{w}}} & \frac{Z_w}{m-Z_{\dot{w}}} & u_0 & 0 \\ M_u & M_w & M_q & 0 \\ 0 & 0 & 1 & 0 \end{bmatrix} \begin{pmatrix} \Delta u \\ w \\ q \\ \Delta\theta \end{pmatrix} + \begin{bmatrix} X_{\delta_T} & 0 & 0 \\ 0 & Z_{\delta_f} & 0 \\ 0 & 0 & M_{\delta_e} \\ 0 & 0 & 0 \end{bmatrix} \begin{pmatrix} \Delta\delta_T \\ \Delta\delta_f \\ \Delta\delta_e \end{pmatrix} \tag{2.20}$$

The differential equations in our dynamics are the horizontal velocity  $\Delta\dot{u}$ , the vertical velocity  $\Delta\dot{w}$ , the pitch rate angle  $\Delta\dot{q}$  and the pitch angle  $\Delta\dot{\theta}$ . The two input controls that will be implemented in the simulation are the elevator  $\Delta\delta_e$  and throttle which controls the propeller power  $\Delta\delta_T$ . The third input  $\Delta\delta_f$  which is flap deflection is not going to be used in the considered design to stabilize the vehicle longitudinally and therefore is set to zero.

### 2.1.3 Ground effect

The Ground effect is a phenomena where changes appear in the aircraft aerodynamics due to it being close to the ground. The ground obstructs the down-wash on the wing effectively from fully developing [6]. The obstruction of the development of the profile around the aircraft imposes three effects. It reduces the down wash angle at the tail and increases the wing body lift and tail lift slopes [9], while also being heavily dependent on the distance the aircraft is from the ground and the form and aspect ratio of the wing [6]. This results in changes in the flow field around the aircraft.

#### General Lifting Line methods:

There are many methods to compute the ground effect influence such as CFD and wind tunnels but the most common one is using numerical lifting line methods and experiments [10]. Over the years many have tried to formulate a dimensionless lift to drag variable that is dependent on geometry of the aircraft and height above ground. The first general formulation come from Weiselberger using Prandtl lifting line methods [6].

$$\frac{(C_{Di}/C_L^2)_h}{(C_{Di}/C_L^2)_\infty} = 1 - \frac{1 - 1.32(\frac{h}{b})}{1.05 + 7.4(\frac{h}{b})} \tag{2.21}$$

The formulation seems to provide similar results to experiments [6] for height to wing width ratio between 0.033 and 0.25. Another formulation for the ground effect is provided by McCormick using Biot-Savart law with horseshoe vortex with span  $\frac{\pi b}{4}$  [6].

$$\frac{(C_{Di}/C_L^2)_h}{(C_{Di}/C_L^2)_\infty} = \frac{(16h/b)^2}{1 + (16h/b)^2} \tag{2.22}$$

These two formulations provide a simple and effective approximation of the ground effect influence over the aerodynamics of the aircraft. By comparing the two formulations as conducted by S.Gudmundsson [6], it could present a good reference for the behavior expected from the aircraft given the height above ground.

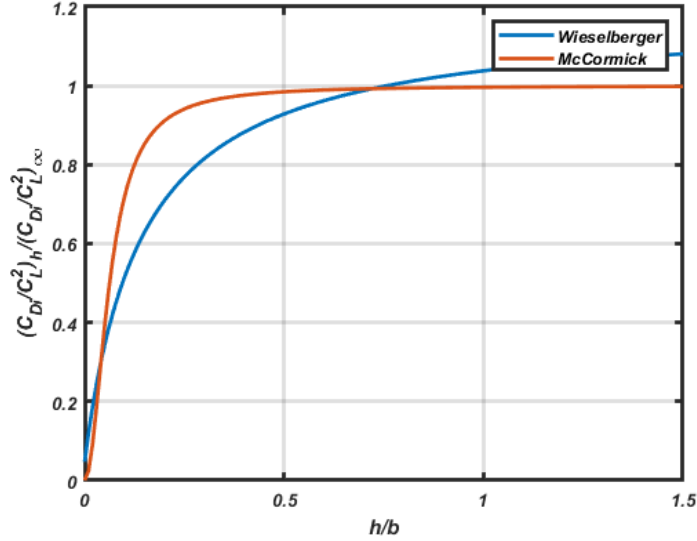


Figure 2.3: Comparison between Weiselberger and McCormick formulations

Discrepancies between the two methods can be seen between 0-0.5 in the height to wing span ratio, as the Weiselberger method is not accurate compared to experiments in that interval. However, the general behavior of a decreasing ground effect influence as the aircraft flies higher and higher above the ground is realistic. There are more accurate methods for ground effect given the wing plan form. The method developed by Philips and Hunsaker is more accurate at predicting the induced drag in ground for several untwisted wings plan-forms. The method uses potential flow algorithm and replaces the ground as a surface with a mirror image of the aircraft as if it is reflected on the ground creating a symmetry across the plane of reflection [10]. The symmetry between the aircraft and its image mirror causes down wash of the aircraft to be offset by an exact up-wash in the mirror image. The combined potential flow of the aircraft and its image is identical to the flow of the potential flow of the aircraft with a ground surface. Since there are several methods for the ground effect based on the vehicle geometry, the one that is considered is the method described by Philips and Hunsaker [10] for tapered wings and small angles of attack is :

$$\frac{(C_{Di}/C_L^2)_h}{(C_{Di}/C_L^2)_\infty} = 1 - \delta_D \exp[-4.74(h/b)^{0.814}] - (h/b)^2 \exp[-3.88(h/b)^{0.758}] \quad (2.23)$$

There  $\delta_D$  is the taper wing correction coefficient for drag:

$$\delta_D = 1 - 0.157(R_T^{0.775} - 0.373)(R_A^{0.417} - 1.27) \quad (2.24)$$

where  $R_T$  is the wing taper ratio while  $R_A$  is the aspect ratio of the wing. The formulation for lift-ground effect influence ratio by Philips and Hunsaker method for tapered wings with small angles of attack:

$$\frac{[C_L(\alpha)]_h}{[C_L(\alpha)]_\infty} = 1 + \delta_L \frac{288(h/b)^{0.787} \exp[-9.14(h/b)^{0.327}]}{R_A^{0.082}} \quad (2.25)$$

There  $\delta_L$  is the taper wing correction coefficient for lift.

$$\delta_L = 1 - 2.25(R_T^{0.00273} - 0.997)(R_A^{0.717} + 13.6) \quad (2.26)$$

## 2.1.4 Vortex Lattice Method

In this section, the main focus will be to provide a general idea of how the vortex lattice method works with some generalized formulas. For an in depth explanation and derivation of the different methods refer to Aerodynamics for Engineers by J.J Bertin and M. L. Smith [11]. The vortex lattice method formulates the planar wing surface on which a grid of horseshoe vortices is super imposed [11]. Using the law of Biot Savart, the induced velocities of each horseshoe is computed at specific control points. The circulation and pressure of the upper and lower wing surface are related to the vortex strengths. The resulting differential pressure over the wing is integrated providing the total forces and moments [11]. The continuous distribution over the surface of the wing is estimated by a finite number of horseshoe vortices as shown in Figure 2.4 .

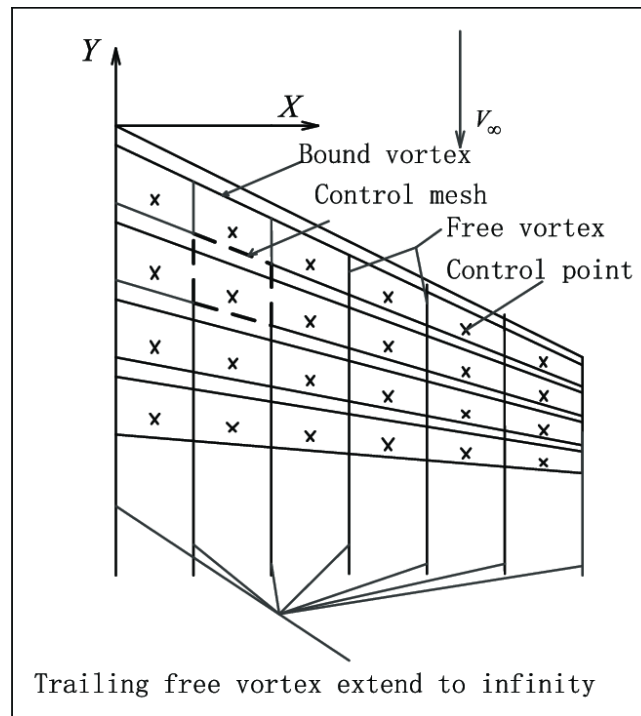


Figure 2.4: Schematic of the classical vortex lattice method by [12].

These horseshoe vortices are placed on trapezoidal finite elements or lattices hence, the method is called vortex lattice. Each panel has a control point as shown in Figure 2.4. These control points are centered span-wise on the three quarter chord line in the middle between the trailing vortex legs in each panel [11]. The measurements of vortex strength is important in this method and one way to approximate it over an arbitrary panel is by the following formula assuming that the flow is parallel to the surface at the control point:

$$\Gamma = \sin(\alpha)2\pi r U_{\infty} \quad (2.27)$$

There,  $\alpha$  is the incidence of the surface relative to the free stream,  $U_{\infty}$  is the velocity of the free stream,  $r$  is the location of the control point where the flow is parallel. The lift per unit span can be computed by the following formula:

$$l = \frac{1}{2}\rho_{\infty}U_{\infty}^2 c 2\pi\alpha = \rho_{\infty}U_{\infty}\Gamma \quad (2.28)$$

While the lift coefficient per section can be derived from Equation 2.28 and calculated according by:

$$C_l = \frac{2\Gamma}{U_\infty c_{av}} \quad (2.29)$$

where  $c_{av}$  is the average chord and it is equal to the area over the span. Assuming a symmetric flow and simple planar wing, the total lift of a group of span units can be approximated by :

$$L = \rho_\infty U_\infty \sum_{n=1}^m \Gamma_n \Delta y_n = C_L q_\infty S \quad (2.30)$$

Where  $n$  is an index for the element,  $\Delta y_n$  is the width of the element. Once the lift per section is derived, the drag can be computed by integrating over the span according to J.J Bertin and M.L Smith [11] with the following relation:

$$C_{D_v} = \frac{1}{s} \int_{-0.5b}^{0.5b} C_l c \alpha_i dy \quad (2.31)$$

there  $a_i$  is the induced incidence angle. The lift to drag ratio can be generalized in numerical formulation through Simpson's rule.

## 2.2 Longitudinal Control System

The initiation of the control system analysis requires knowledge about the dynamics of the system. With the help of literature on control theory, the stability and performance of the open loop system will be analyzed and the feasibility of three closed loop methods will be studied as well. In this section, the main parameters that are used to measure the performance of the control system is studied as well as the mathematical formulation of the different methods.

### 2.2.1 Initial Control Analysis

The dynamic system is outlined in Section 2.1.2 with the linearized Equations of Motion (EOM) in Equation 2.20. The general formulation for the linear dynamic system as a first order Ordinary Differential Equations (ODE) is :

$$\begin{aligned} \dot{x}(t) &= Ax(t) + Bu(t) \\ y(t) &= Cx(t) + Du(t) \end{aligned} \quad (2.32)$$

Also called state space form in continuous time [13]. This is an advantageous formulation as a lot of methods in control theory uses it , in addition to the fact that it will simplify the implementation using Matlab. Another useful formulation is the transfer function  $G(s)$  in ( $s$ ) domain. It also helps with the implementation and requirement of different methods. To change the formulation from the state space to transfer function, the following equation is used:

$$G(s) = C(sI - A)^{-1} B + D \quad (2.33)$$

It can be seen from the dynamic system that it is a multi-input multi-output system. Two inputs which are the throttle/propeller and the elevator angle and four outputs which are the horizontal and vertical velocity, pitch rate and pitch angle. When working with dynamic systems, it is important to check the possibility of formulating the input/output relation in even lower dimensions. That is called minimal realization. The state space representation of the system is said to be in minimal realization if it is

both observable and controllable. Glad and Ljung in [13] outline the definitions of these conditions which are :

$$S(A, B) = [B \ AB \ A^2B \ \dots \ A^{n-1}B] \quad (2.34)$$

$$O(A, C) = \begin{bmatrix} C \\ CA \\ \cdot \\ \cdot \\ CA^{n-1} \end{bmatrix} \quad (2.35)$$

The theorems states that for the system to be controllable, the row vector  $S(A, B)$  has to be full rank. Similarly, for the system to be observable the column  $O(A, C)$  has to be also full rank. These concepts describe the influence from the input on the state space vectors and how it affects the outputs. After checking if the system is minimized to the smallest dimension, some stability studies can be started. The basic one in control theory is the eigenvalues of the transfer function defined in Equation 2.33. For **Single Input Single Output (SISO)** systems the bode plot is important as it can provide a lot of insight on the properties of the system and its gain [13]. However, for **Multi Input Multi Output (MIMO)** systems,  $G(s)$  is a matrix and even though the bode plot for inputs and outputs can be plotted, it will not display the connections between the different subsystems [13]. That is why the singular values are also investigated as a second parameter for stability, since the interaction and direction of poles and zeros is an important factor for amplification. They are often calculated through factorization of matrices also called **Singular Value Decomposition (SVD)**.

$$A = U\Sigma V^* \quad (2.36)$$

This measures and quantifies the upper and lower bound of the gain in the **MIMO** system over the frequency domain. Since in **MIMO** the direction of the poles and interaction between the different inputs and outputs is an additional important aspect that has to be kept in check. The interpretation is that an input with direction  $V$  leads to an output of direction  $U$ , and  $\Sigma$  is the scaling. The definition of the system amplification is therefore defined by Equation 2.37.

$$\underline{\sigma} \leq \frac{|y|}{|x|} \leq \bar{\sigma} \quad (2.37)$$

there  $\sigma$  is the singular value of the dynamic system  $A$ . The main focus is to check the highest amplification  $\bar{\sigma}$  and lowest amplification  $\underline{\sigma}$ . For the performance analysis of the system, it is useful to define some concepts that will be used such as step response and impulse response. There the step response represents the behavior of the output over time when input changes from 0 to 1 in a very short time. There are many parameters that can be measured from the step response of the system and these parameters are used to check the performance of the control system. The first one is the rise time of the output which demonstrates how fast is the system reacting to the changes in the input and it is measured as the time it takes the output to rise from initial value to 70% of the final value. The overshoot represents the accuracy of the system to reach the final value, it is generally measured as how inaccuracies in the response are expected to display in the output before it corrects itself. This parameter is commonly used as percentage of the final error but in this project the absolute value of the error is used instead as in some cases the final state will be at zero. Taking the percentage of error

in respect to zero can be misleading. The final parameter is the settling time and it represents how long it takes the system to settle completely into the final value.

## 2.2.2 Pairing Problem and Decentralized Control

The simplest approach to control systems in the MIMO case is the decentralized approach. The method builds on the idea of connecting one input to one output. according to the following equation:

$$u^i = F_r^i r_j + F_y^i y_j \quad (2.38)$$

where the  $F_y$  matrix is going to be diagonal which indicates which input is coupled to which output.

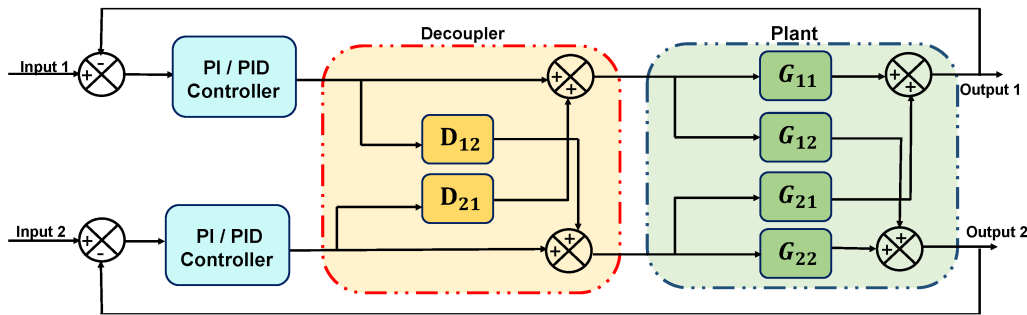


Figure 2.5: Typical decentralized decoupled two inputs two outputs closed loop [14]

The ideal situation for this method as it can be seen from the description is the square system where the number of inputs are equal to the number of outputs which is not the case here. However, the computations using this method can help in understanding the requirements of the system. The interaction between the inputs and the outputs is an important factor as it provides a good parameter to choose which coupling the system requires. This is called the pairing problem. The measurements used to check this parameter is the **Relative Gain Array (RGA)** and it can be computed through the following equation:

$$RGA(A) = A .* (A^{-1})^T \quad (2.39)$$

Where  $(.*)$  is an element-wise multiplication: it checks the direct amplification and relation between each input to each output. To determine that the following coupling is appropriate, the relative gain array of the system is computed at zero frequency and the cross frequency. After computing the **RGA** matrix at these two frequencies the elements which are positive in the **RGA** matrix are the ones that have feasible coupling. The negative frequencies could lead to uncertainties in some frequencies. The diagonal of the **RGA** at the cross frequency elements are also expected to be as close as possible to a value of 1 otherwise bad performance in the closed loop system is expected.

It is also useful to check the internal stability of the system since the approach for decentralized controller is the idea of several **SISO** systems connected. This stability represents the input output stability of the system. This is studied through the sensitivity and the complementary sensitivity of the system. Those two concepts can help in analyzing the system behavior further. The first concept is sensitivity  $S$  which quantifies the sensitivity of the closed loop system to model changes.

$$S = (1 + GF_y)^{-1} \quad (2.40)$$

Which describes the feedback through two boundaries, disturbance attenuation when  $|S(i\omega)| < 1$  and

disturbance amplification when  $|S(i\omega)| > 1$ . The complementary sensitivity  $T$  quantifies the ability of the closed loop to reject disturbances and suppress the impact of model errors.

$$T = (1 + GF_y)^{-1}GF_y \quad (2.41)$$

The relation between the two aforementioned functions is:

$$S + T = 1 \quad (2.42)$$

This formulation helps with the tracking of uncertainties and problematic frequencies in the system. The decentralized controller has hard requirements on these parameters as the internal stability of the system can affect the relations between the input and outputs.

### 2.2.3 H-infinite Robust Control

#### Uncertainty Model and Stability:

The robust control approach focuses mainly on robustness in the face of model uncertainty. This is an appropriate approach when control systems are simulated through software as it guarantees a certain performance even if the approximated model is not completely accurate. This requires the uncertainty to be modeled into the system as a parameter to be taken into account. The theoretical model of uncertainty in closed loop is shown in Figure 2.6.

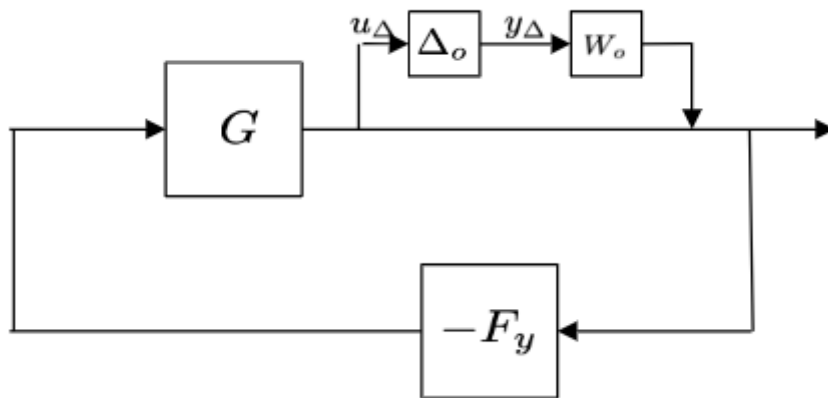


Figure 2.6: Modeled uncertainty in closed loop system.[13]

There,  $\Delta$  is the perturbation matrix model with the same dimension as the  $G(s)$  that is set on the output side, and  $W_0$  is the uncertain weight function. The system is described as robust by proving that the same system with the modeled uncertainty in Figure 2.6 is stable for all perturbations  $\Delta_0$ . To derive the proof of stability in all perturbations, the Small Gain Theorem is described by T. Glad and L. Ljung [13], which states that if two open loop systems and their loop gains are both input-output stable then the interconnection of these systems in a closed loop is also stable. The input-output stability condition is formulated in Equation 2.43 where it describes that the system is stable if the system gain is bounded [13].

$$\|S\| < \infty \quad (2.43)$$

The second condition is for the loop gain of both open loop systems to be stable which means the product of both gains has to be less than 1 as defined in Equation 2.44

$$\|S_1\| \|S_2\| < 1 \quad (2.44)$$

After defining what the stability for an uncertain system is, the requirements for this stability are derived, by formulating the loop from  $\Delta y$  to  $\Delta u$ , as described by T. Glad and L. Ljung [13]. The final result of the derivation leads to the following condition :

$$\|TW_0\|_\infty < 1 \quad (2.45)$$

### H-infinite controller Theory :

The general theory behind  $H_\infty$  controllers, is mainly minimizing singular value concept described in chapter 2.2.1, where the system gain is dampened over the maximum gain (singular value) of  $G_{ec}(iw)$  [13]. There the  $ec$  stands for extended closed loop shown in Figure 2.7.

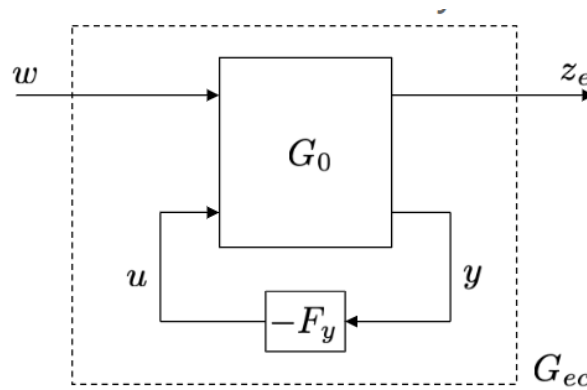


Figure 2.7: Block diagram for the extended closed loop system [15]

From the block diagram in Figure 2.7 the input to output relation is:

$$z_e = wG_{ec} \quad (2.46)$$

That leads to reduction in the high problematic system gain in the open loop. This is applied through weight functions which help reduce the system gain in certain areas in the frequency spectrum. The search for the controller is done according to [13]:

$$\|G_{ec}\|_\infty \leq \gamma \quad (2.47)$$

If this inequality holds then it follows that

$$\begin{aligned} |W_S S| &\leq \gamma \\ |W_T T| &\leq \gamma \\ |W_u G_{wu}| &\leq \gamma \end{aligned} \quad (2.48)$$

The first weight function is generated from the sensitivity function to penalize sensitivity to noise written as  $W_S$ . The second one is  $W_T$  generated from the complementary sensitivity function to track and reject disturbances. It acts as a low pass filter for performance improvement. Third function is  $W_u$  to control the inputs magnitude within the system and it is a high pass filter. In the inequalities

in Equation 2.48, the weights functions  $W_S, W_T, W_u$  are used to bound the important singular values in the closed loop system [13]. These weights are modeled as the general weight matrix  $W_0$  from the condition in Equation 2.45. The minimization problem can be formulated based on the Equation 2.46. The signal minimization problem and the system norm problem are equivalent:

$$\min_{F_y} \sup_w \frac{\|z_e\|_2}{\|w\|_2} = \min_{F_y} \|G_{ec}\|_\infty \quad (2.49)$$

Where  $F_y$  is formulated by the weights functions for the function of the closed loop system:

$$F_y = \arg \min_{F_y} \left\| \begin{array}{c} W_S S \\ W_T T \\ W_u G_{wu} \end{array} \right\|_\infty \quad (2.50)$$

## 2.2.4 Infinite time Optimal Control

Optimal control is a very advantageous method to design control systems as it offers a systematic approach to the problem with reformulation to make it into a quadratic optimization problem [16]. The general formulation for optimization problem in continuous time is the following:

$$\min \phi(x(t_f)) + \int_{t_i}^{t_f} f_0(x(t), u(t)) dt \quad \text{s.t.} \quad \begin{cases} \dot{x}(t) = f(x(t), u(t)), \\ x(t_i) = x_i, \\ u(t) \in U, t_f \geq 0. \end{cases} \quad (2.51)$$

There, the  $\phi(x(t_f))$  is the terminal cost and  $t_i$  and  $t_f$  are the initial and terminal times. The end state  $x(t_f)$  is free and can end up with any value in  $R^n$ . The main concept is to find control  $u$  that will transfer the initial state  $x(t_i)$  to the terminal state  $x(t_f)$  while keeping the cost function as small as possible. The application for control systems where the main objective is to maintain a certain position for a long period, despite disturbances is common and mainly referred to as the infinite time horizon optimal controllers. The general formulation for such problem can be derived from Equation 2.51 as follows:

$$\min \int_0^\infty f_0(x(t), u(t)) dt \quad \text{s.t.} \quad \begin{cases} \dot{x}(t) = f(x(t), u(t)), \\ x(t_i) = x_i, \\ u(t) \in U, \end{cases} \quad (2.52)$$

where  $f$  and  $f_0$  are locally differentiable continuous functions. The main objective is to control the system in an equilibrium state. This is needed to be able to obtain finite cost [16]. It is important to define two key concepts. The first one is the autonomous systems which is a classification for Ordinary Differential Equations. The definition is that if the independent variable does not appear explicitly in the system, then it is an autonomous system [17]. The second term is the equilibrium point in the context of infinite time horizon controllers. The state  $x^*$  is said to be in equilibrium if the function  $f(x^*) = 0$  with the property that if it starts in  $x^*$  it remains in  $x^*$  [16]. Before solving the problem in Equation 2.52, a number of assumptions has to be set. The assumptions are :

- The artificial output of the system at  $f_0$  is observable at  $(C,A)$  and controllable at  $(A,B)$  in accordance to the definition provided in Section 2.2.1.
- The cost function  $f_0$  is positive semi definite for all  $(x,u) \in R^{n \times m}$  and positive definite when  $u \neq 0$ .

Now for an optimal quadratic control problem, it can be formulated as follows:

$$J^*(x_0) = \min \int_0^{\infty} x^T Qx + u^T Ru dt \quad \text{s.t.} \quad \begin{cases} \dot{x}(t) = Ax + Bu, \\ x(0) = x_0, \\ Q = C^T C, R > 0 \end{cases} \quad (2.53)$$

There  $f_0 = x^T Qx + u^T Ru$  where  $R$  is the disturbance intensity over the input  $u$ . Both  $R$  and  $Q$  have to be positive for the assumptions to hold. Now the value function  $J^*(x, u)$  can be defined. Since both the cost function  $f_0$  and dynamics  $f$  are both autonomous which means not explicitly dependent on time then the value function will be the same. The value function is defined by Theorem 9 [16] by the **Hamiltonian Jacobi Bellman Equation (HJBE)**, given that the assumptions mentioned before and two conditions in the Equation 2.54 hold. Then the value function  $V = J^*(x, u)$  and the  $\mu(x)$  is an asymptotically stabilizing feedback control.

$$\begin{aligned} \underbrace{\min}_{u \in U} [f_0(x, u) + \frac{dV}{dx}(x)^T f(x, u)] &= 0 \\ \mu(x) &= \underbrace{\operatorname{argmin}}_{u \in U} [f_0(x, u) + \frac{dV}{dx}(x)^T f(x, u)] \end{aligned} \quad (2.54)$$



# Chapter 3

## Methodology

The layout of the process for the project is shown in Figure 3.1. The project starts with defining the state where the ground effect vehicle has to be stabilized over a wavy surface and ends with results comparison of both the aerodynamic data and the performance of the control systems.

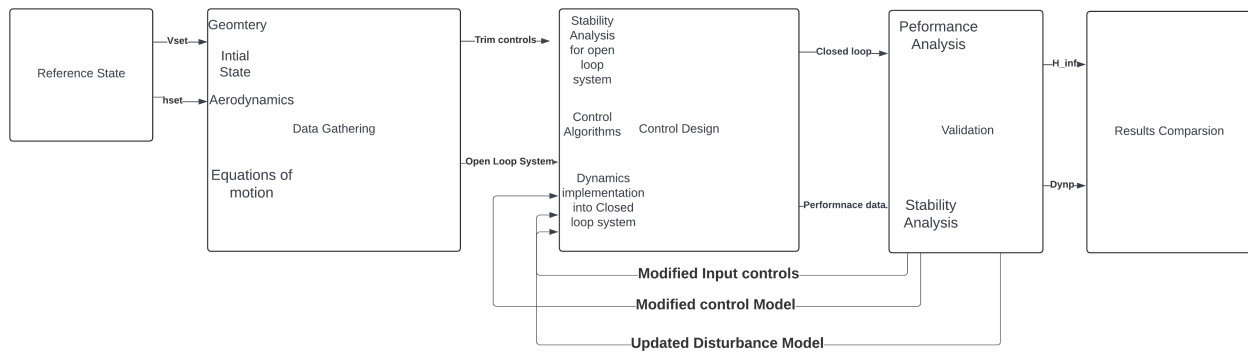


Figure 3.1: Workbench layout for the method

### 3.1 Research Process and Gathering Data

In this section, the main focus is on the process of building and using the models that contribute to the final results. The inputs and the assumptions that are used when computing the final data will be shown and validated along the way with as much detail as possible to ensure repeatability.

#### 3.1.1 Aerodynamics: Lifting Line Method

##### Geometry

The main software used in this method is the nonlinear lifting line library in Matlab developed by KTH. The main inputs to compute the aerodynamic data for the GE vehicle is the geometric data. The first ones are wing and tail airfoils. The airfoils are identified through the design report [7], as K3311 for the wing and NACA0008 for the tail [7], both shown in Figure 3.2 and Figure 3.3. The aerodynamic data for these airfoils is also needed as inputs for the LLM library. Xfoil software is used to analyze these airfoils.

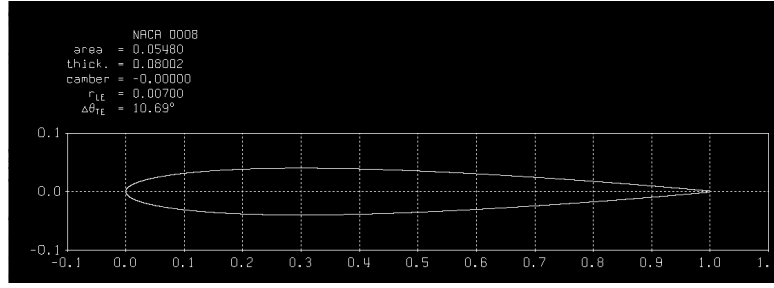


Figure 3.2: Airfoil for the tail NACA0008

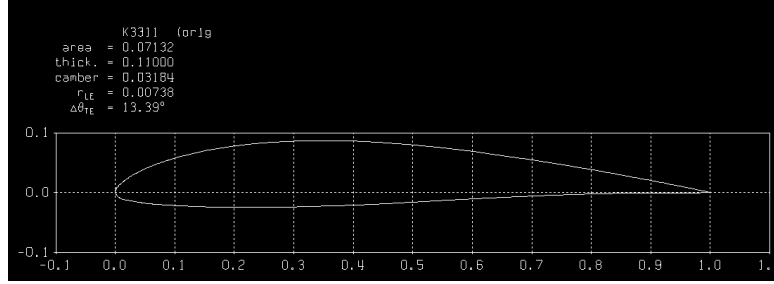


Figure 3.3: Airfoil for the wing K3311

The data for airfoils is analyzed at three different Reynolds number which are  $3 \times 10^5$ ,  $7.5 \times 10^5$ ,  $1 \times 10^6$ . The second focus is on the tail as it is the elevator and it helps finding the trim condition for the GE vehicle later. In the analysis two elevator settings are studied in Xfoil which are  $-10^\circ$  and  $10^\circ$ . The flap is set at coordinates  $x/c = 0.8$  and  $y/b = 0$ . Another important input to the GE vehicle is the neutral point, which is based on the estimation from the weight distribution [7], and given a reasonable initial estimation for a static margin of 16 % [6].

Table 3.1: Preliminary data

Preliminary Data		
Parameter	Wing	Tail
$AR$	3.2961	3.1347
$C_{L\alpha}$	2.161	2.09
$V_H$	-	0.36
$V_V$	-	0.05
$b$	1.73	0.73
$S$	0.908	0.17
$\frac{\partial \epsilon}{\partial \alpha}$	0.477	0.339
Neutral Point = 0.1915 m		

In Table 3.1,  $V_V$  and  $V_H$  are the volume ration of the vertical tail and the horizontal tail [7]. The  $AR$  is the aspect ratio,  $b$  is the span of the wing,  $S$  is the reference area and  $\frac{\epsilon}{\alpha}$  is the induced downwash. These parameters are computed by formulation from B.Etkin [9]. The moments of inertia  $I$  need to be approximated here for a correct estimation of the the aerodynamics together with the data obtained from Xfoil as mentioned in the geometry section. The fuselage in this case is assumed to be a cylinder when computing the moments of inertia  $I$  [ $kgm^2/s$ ]. The moments of inertia obtained are :

$$I = \begin{bmatrix} 0.43 & 0 & 0 \\ 0 & 1.21 & 0 \\ 0 & 0 & 1.62 \end{bmatrix} \quad (3.1)$$

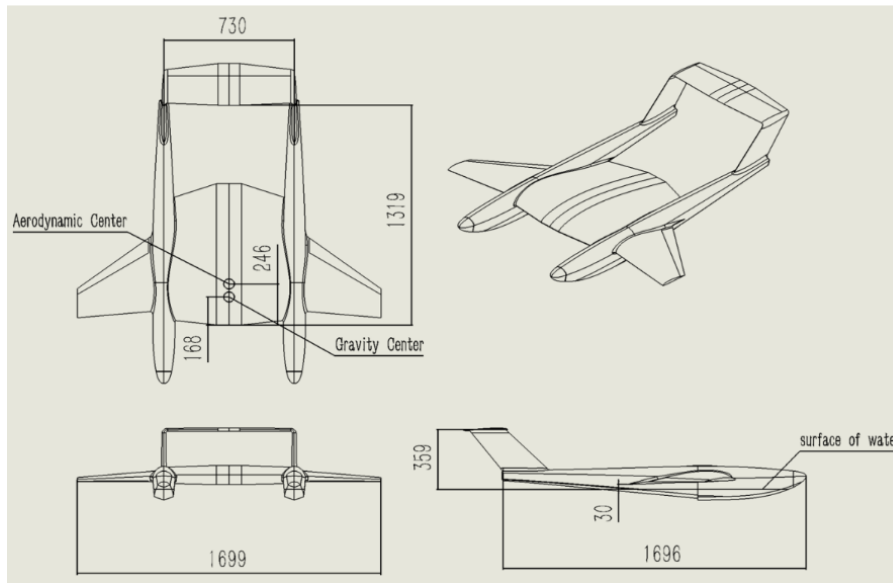


Figure 3.4: 3-view drawing [7]

Another important geometric feature in the GE vehicle is that it has a twist angle of  $3.5^\circ$  on the wing and  $0.5^\circ$  on the tail [7]. These are crucial parameters as they affect the pitching moment and the static stability of the vehicle.

### Ground Effect Model

The model used for the ground effect is based on the prediction formulas derived by W.F Philips [10]. The formulation used is the taper wing lift to drag ratio for small angles of attack formula shown in Section 2.1.3. These formulations are coded into Matlab functions to be used in the nonlinear lifting line model based on geometric data of the GE vehicle and the height above the ground. In theory, the ground effect makes the vehicle generally more efficient as the induced drag is reduced and the lift is slightly increased. To validate the model, the behavior of lift and drag is checked with the geometric data in table 3.1 and shown in the Figure 3.5:

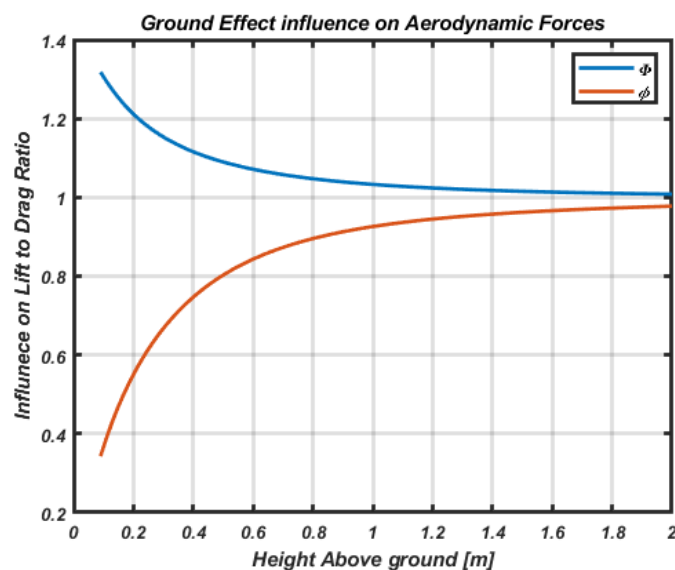


Figure 3.5: Influence on the aerodynamics forces

There the value  $\phi$  is the ground effect influence factor for induced drag and  $\Phi$  is the ground effect influence factor for lift. The ground effect influence is computed from height  $2 > h > 0.09[m]$  as the model is only accurate when the height is above 0.09 [m] [10], while for heights above ground of less than 2 [m], the ground effect tends to be negligible as shown in 3.5. At heights less than 0.09 [m] the extreme ground effect occurs and it is not possible to predict the effect on the lift to drag ratio in that region without more sophisticated software like CFD. For that it is assumed that when the vehicle gets close to 0.1[m] to the ground then the controller has already failed and it will try to stay outside of that margin. The behavior of the aerodynamic forces based on the proximity of the aircraft to the ground is appropriate based on the theoretical formulas that are seen in Section 2.1.3. This can be further validated by comparing them to the graphs done by W.Philips [10]. For simulating the wavy surface the model from K.V. Rozhdestvensky [18] is used, as follows:

$$h^*(x, t) = 1 + \theta x - a_w \cos[k(x \cos \beta + z \sin \beta + t \cos \beta)] \quad (3.2)$$

where  $a_w$  is the amplitude of the wave,  $\theta$  is the angle of the pitch and  $\beta$  is the course angle on the horizontal plane. This represents the gap between the wing and the underlying surface, as shown in Figure 3.6:

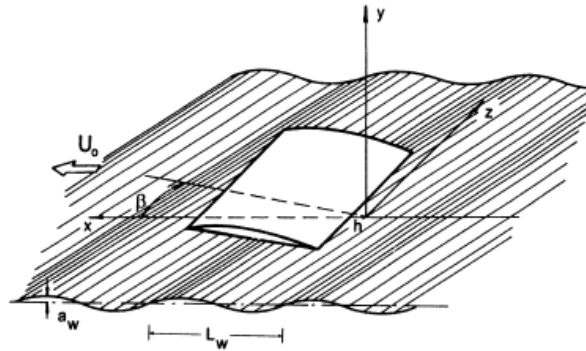


Figure 3.6: A lifting surface moving in proximity to the wavy ground from Rozhdestvensky [18]

This wavy surface will be used to simulate the changes and disturbances that occur in the aerodynamic forces of the wing, as shown in Figure 3.5. The intensity of the disturbances in the aerodynamic data can be controlled by decreasing the period of the waves  $T_{wave}$ . The model in Equation 3.2 computes the ground effect over the surface, then the changes in lift to drag ratio are averaged and included in the lifting line data model to account for the ground effect. Since the region where the computations are conducted have no extreme ground effect, it is safe to assume that the average of the disturbed influence is an appropriate approximation. To validate the model, the wavy surface behavior is checked together with the ground effect influence variations. The expected behavior as explained in theory by Gudmundsson [6] is that the waves cause a small increase and decreases in the lift to drag ratio and ground effect influence factor. In Figure 3.7 the behavior is displayed. As expected, the highest GE influence occur when the wing is closest to the surface and the influence is minimal when the height above the ground is at its peak.

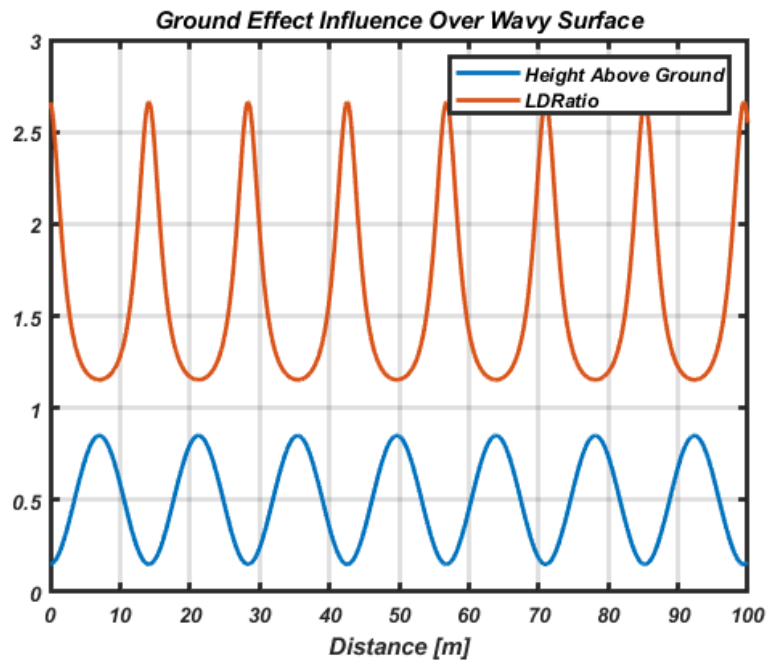


Figure 3.7: Ground effect influence on the wing above surface

### Lifting Line model

After modeling the ground effect and including it into the flight simulator library by KTH. The LLM is used to approximate the aerodynamics of the aircraft. The first geometric parameters, needed are the leading edge points on the wing and tail. These define the shape of the wing in the simulation together with the cord and span of both wing and tail. These leading edge points will be used as explained in Section 2.1.1. The aerodynamic data obtained from Xfoil shown in Figure 3.8 and Figure 3.9, the red point is the maximum LD for each airfoil. The model uses this data from the airfoils together with the geometry of the vehicle to compute the aerodynamics on the whole aircraft. Then LLM model uses the data for the tail with elevator deflection  $-10^\circ$  and  $+10^\circ$  from Xfoil as well to determine the aerodynamics of the aircraft in different trim sets.

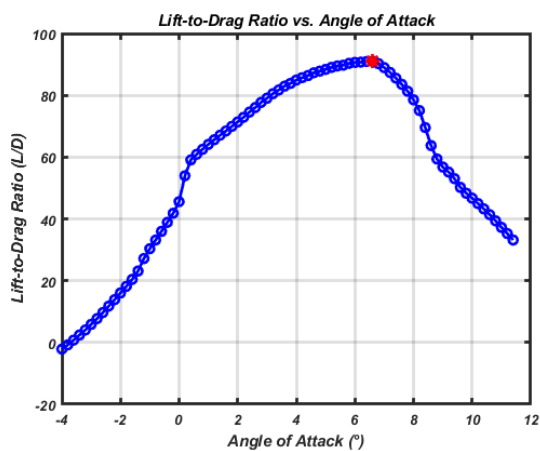


Figure 3.8: The lift to drag ratio (LD) for Airfoil K3311 at Reynolds number = 350000.

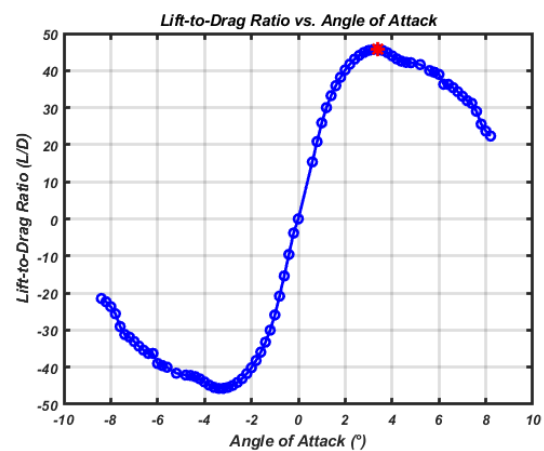


Figure 3.9: The lift to drag ratio (LD) for Airfoil N0008 at Reynolds number = 350000.

### 3.1.2 Aerodynamics: Vortex Lattice

After defining the reference state and the geometric data such as tail and wing airfoils as well as mass and center of mass, another method to compute the aerodynamics of the wing is used, and compared with the LLM to ensure validity. The method is VLM, and to implement it, an off-the-shelf software like Xflr is used to simulate and compute the aerodynamics of the vehicle with the inbuilt ground effect functions. It is important to note that Xflr uses Xfoil to determine the aerodynamics of the airfoils, so for this method the figures 3.8 and 3.9 are valid as well. The first step is to divide the wing into two sections as the used wing in the vehicle is a compound wing. The first section represents the inner part of the wing and the second is the outer part. The measurements given for the cord at the tip and the root from the design report [7].

Table 3.2: GE vehicle wing geometry

GE vehicle Wing Geometry [m]		
Part	Wing	Cord
Inner Root	0.0	0.85
Inner Tip	0.365	0.714
Outer Root	0.365	0.5
Outer Tip	0.865	0.175

With an incidence in the wing of  $3.5^\circ$ . Tail is made up of one section with root cord of 0.286 [m] and tip cord of 0.214 [m]. The exact position of the tail is not given, so it was approximated based on the drawings in Figure 3.4, at 1.696 [m] behind the wing and 0.3 [m] above the wing with an incidence of  $0.5^\circ$ . Before being able to analyze the vehicle, airfoil data has to be gathered by doing analysis on the airfoils first. For that the analysis on the airfoils of both tail and wing is done using Reynolds numbers from  $8 * 10^4$  to  $3 * 10^6$  with 72 Reynolds numbers in this interval. This analysis is also done on the tail with elevator angles [-10, -4, -2, -1, 0, 2, 4, 6, 8, 10]. The vehicle is analyzed given a speed of 18 m/s and in the angles of attack between  $[-5^\circ, 5^\circ]$  in ground effect with 0.5 m above the ground. The flows shown in Figure 3.10:

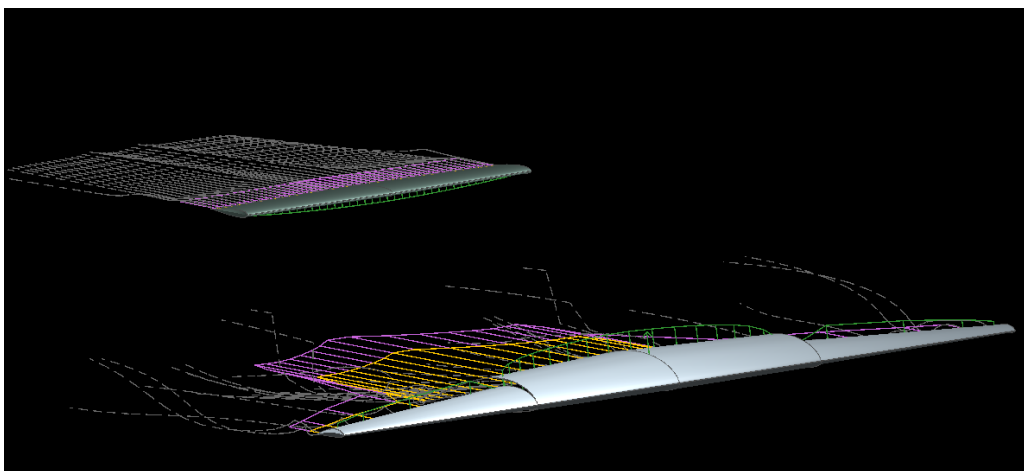


Figure 3.10: 3D plane view in XFlr

The same analysis is conducted for all the elevator trim sets between  $[-4^\circ, 10^\circ]$ . The data is compared with the one from LLM. The aerodynamic data from these methods will be used in the flight simulator which is the main tool for the design process of the control systems later on.

## 3.2 Flight Simulator and Open Loop System

### 3.2.1 Flight Simulator

The flight simulator is built to simulate the motion of the GE vehicle. The main model is built with 9 EOM. Since this is a longitudinal study, the focus is on the 2D motion and only 9 out of the 12 EOM which is shown in 2.1.2. The system of differential equations is represented by seven variables and two control variables. The seven variable are computed with the following reformulated EOM:

$$\begin{aligned}
 \dot{u} &= \frac{\Delta X}{m} - g\Delta\theta\cos\theta_0 - q_0w \\
 \dot{w} &= \frac{\Delta Z}{m} + g\Delta\theta\sin\theta_0 + q_0u \\
 \dot{q} &= \frac{\Delta M}{I_y} \\
 \dot{\theta} &= q \\
 \dot{x}_e &= \cos(\theta)u + \sin(\theta)w \\
 \dot{z}_e &= \sin(\theta)u - \cos(\theta)w \\
 \dot{m} &= 0
 \end{aligned} \tag{3.3}$$

there the forces  $\Delta X$  and  $\Delta Z$  and the pitch moment  $\Delta M$  are calculated by :

$$\begin{aligned}
 \Delta X &= T - D\cos(\alpha) + L\sin(\alpha) \\
 \Delta Z &= -L\cos(\alpha) - D\sin(\alpha) \\
 \Delta M &= (q_{dyn}S_{ref}C_p(C_m + \frac{C_{m\dot{\alpha}}\dot{\alpha}C_p}{2V_\infty} + T) + \Delta X x_{CG} + \Delta Z x_{CG}) \\
 \dot{\alpha} &= (\cos(\alpha)^2(\dot{w}u - w\dot{u}))/u^2
 \end{aligned} \tag{3.4}$$

There the  $L, D, C_m$  and  $C_p$  are obtained from the aerodynamic data provided by LLM and VLM together with the initial state  $x_0$ . The thrust  $T$  is a scaling of the propeller power, and in this case it is assumed to be 30 % of the gravitational force of the vehicle  $mg$ ,  $x_{CG}$  is the location of the center of gravity,  $q_{dyn}$  is the dynamic pressure,  $S_{ref}$  is the reference area,  $V_\infty$  is the airspeed in [m/s], and  $C_{m\dot{\alpha}}$  is the change increment of the moment with respect to the angle of attack  $\alpha$ . The formulation of the forces and moments is based on the model from Stevens, Lewis and Johnson in Aircraft Control and Simulation [19]. The simulator is tested to find the trim condition by solving the ODE given the reference cruise state. With the help of the flight simulator and the dynamical system, it is possible to study the flight modes and the open loop system stability by first checking the root locus for the different flight modes. The two flight modes that are important in longitudinal stability are the short period and the phugoid. The short period being seen as the motion where oscillations of angle of attack are close in magnitude and phase to pitch rate with small and negligible variations in speed [9]. The phugoid is the opposite of short period where the variations in angle of attack and pitch rate are small while the variations in speed are larger.

### 3.3 Control Design Methods

After using the system of ODE to determine the trim condition and the linearized dynamic system in Equation 2.20, the data gathered from the open loop system can help in the design of the closed loop system. Mainly two approaches will be tested and compared at the end. The decentralized controller with simple PI controllers approach will be analyzed to study input to output interaction which is useful to evaluate the performance of the system but it is not the main focus. This approach is simple to implement, but has extra requirements on the stability of the system. The second one is robust controllers, and they tend to be most effective when model uncertainties are present by defining margins to the stability conditions. Optimal controllers have the most systematic approach to minimize the effort by the system while stabilizing it. The formulation for the optimization problem starts by transferring from the state space to transfer function representation. This allows the using of a wide library of inbuilt commands in Matlab which will make the analysis process simpler. The transfer from state space to transfer function is explained in Section 2.2.1. The first check before starting the design of a feedback closed loop system, is that the system is in minimal realization state, where it is observable and controllable. The controllability and observability conditions are mentioned in Section 2.2.1. The Matlab inbuilt commands are used to compute the open loop observability and controllability matrices which are *ctrb* and *obsv*. The rank of these matrices is the same as the rank of the dynamic system (*A* matrix in state space), which means the system fulfills these conditions.

#### 3.3.1 Pairing Problem and Decentralized Controller

Start by providing some main assumptions for the system. The main assumption is that decentralized controllers are not meant to operate non-square systems where the number of inputs is not the same as the number of outputs. The considered system has two inputs and four outputs as shown in Equation 3.21:

$$\begin{Bmatrix} \Delta \dot{u} \\ \Delta \dot{w} \\ \Delta \dot{q} \\ \Delta \dot{\theta} \end{Bmatrix} = \begin{bmatrix} -0.0729 & 0.1994 & -0.1419 & -9.8096 \\ -1.0389 & -5.6416 & 15.6779 & -0.0888 \\ -0.2151 & -9.4656 & -36.6299 & 0 \\ 0 & 0 & 1 & 0 \end{bmatrix} \begin{Bmatrix} \Delta u \\ w \\ q \\ \Delta \theta \end{Bmatrix} + \begin{bmatrix} 0.0002 & 0.0051 \\ -0.0211 & 0 \\ -0.2018 & 0.0191 \\ 0 & 0 \end{bmatrix} \begin{Bmatrix} \Delta \delta_T \\ \Delta \delta_e \end{Bmatrix} \quad (3.5)$$

For that, the decentralized controller design is not feasible but it is still useful as it provides further analysis on the interactions between the inputs and outputs. Mainly solving the pairing problem to check the sensitivity between each input and output. The pairing problem has to be solved as mentioned in Section 2.2.1. The RGA is calculated first for the whole non square dynamic system with transfer function *G*, by using the formula in Equation 3.6

$$RGA(G(i\omega)) = G(i\omega) \cdot *(G(i\omega)^{-1})^T \quad (3.6)$$

Since this is not a square system, the command *pinv* is used to determine the inverse which is a pseudo inverse operator. As explained in Section 2.2.1, the rules for evaluating how good the solution with respect to the performance is first the sum of all rows has to be equal to 1 for the system to be feasible. Second rule is avoid choosing the pairing that has a negative RGA. The third and final rule is that the diagonal of the RGA has to be close to 1. This corresponds to large amplifications between input and outputs [13]. Now to design a PI controller, it is required to define the performance properties of that controller that will contribute to the design process of the control. The phase margin for said controller and its cross frequencies are important parameters as stability margins for the system. The

cross frequency is set to  $\omega_c = 0.1$  and phase margin  $\varphi_m = \frac{\pi}{3}$ . The designed PI controller is based on the following formulation :

$$f_{ij} = K_j \left(1 + \frac{1}{sT_{ij}}\right) \quad (3.7)$$

with the loop gain being  $L = GF$ , so the components of  $L$  which are  $l_{11}$  and  $l_{12}$  have to fulfill the specifications and stability margins defined. The value  $T_{ij}$  can be determined through the minimum phase margin and evaluated  $\arg(g_{11}(i\omega))$  from the Bode plot through Equation 3.8

$$\arg g_{11}(i\omega_c) + \arctan(\omega_c T_{i_1}) - \pi/2 - \varphi_m = -\pi \quad (3.8)$$

Now find the loop gain components with  $T_{ij}$ :

$$l_{11}(s) = g_{11}(s) \left(1 + \frac{1}{sT_{ij}}\right) \quad (3.9)$$

where now  $K_j$  can be computed with  $l_{11}(s)$ :

$$K = \frac{1}{l_{11}(i\omega_c)} \quad (3.10)$$

there  $l_{11}(s)$  is evaluated in the Bode plot.

### 3.3.2 Robust $H_\infty$ Controller

After providing a definition to the extended system where the weights defined in Section 2.2.3, are computed and the new block diagram system as shown in Figure 2.7, the weights are used to augment the plant/system into an extended system. To determine these weight functions there are two approaches, the first one is starting by designing a simple stable feedback loop system and then implementing robustness measures with the augmentation/weight functions by inspecting the generated gain and applying weights on the needed frequencies. This is the loop shaping approach based on the performance of the initial feedback loop. This can require multiple iterations as the performance parameter will have to be set and then requirements have to be derived each time. The second approach is solving the signal minimization problem:

$$\min_{F_y} \sup_w \frac{\|z_e\|_2}{\|w\|_2} = \min_{F_y} \|G_{ec}\|_\infty \quad (3.11)$$

which corresponds to minimizing the  $H_\infty$  norm of the  $G_{ec}$ . The method has no direct solution. Instead it sets a low initial value on the performance parameter  $\gamma$  and it solves the Riccati Equation 3.15 given the state space of the extended open loop system  $G_e$  which is shown in 3.12.

$$\begin{aligned} \dot{x} &= Ax + Bu + N\omega \\ z &= Mx + Du \\ y &= Cx + \omega \end{aligned} \quad (3.12)$$

there A, B, C are already defined in Section 3.3.1.  $N = I$  with size  $4 \times 4$ , and  $M$

$$M = \begin{bmatrix} s+0.0729 & 0.1994 & 0.1419 & 9.81 \\ 1.0389 & s+5.6416 & -15.6779 & 0.0888 \\ 0.2151 & 9.4656 & s+36.6299 & 0 \\ 0 & 0 & -1 & s \end{bmatrix} \quad (3.13)$$

Now only one condition is left before solving the Algebraic Riccati Equation (ARE), and that is to check if the observer  $A - NC$  is stable. The inbuilt *eig* command in Matlab is used providing the following eigenvalues :

$$eig(A - NC) = \begin{bmatrix} -31.9820 + 0.0000i \\ -11.3595 + 0.0000i \\ -1.0293 + 0.5183i \\ -1.0293 - 0.5183i \end{bmatrix} \quad (3.14)$$

As it can be seen from the equation, all the real parts of the eigenvalues are in the left hand side, which means the observer in this case is stable. Now the ARE is solved to determine a positive definite solution  $S$  given a  $\gamma$ .

$$A^T S + SA + M^T M + S(\gamma^{-1} NN^T - BB^T)S = 0 \quad (3.15)$$

There it will iterate until the  $\gamma$  is as low as possible which will lead to an optimal  $H_\infty$  controller. The indirect solution method leads to a formulation of the closed loop controller in terms of feedback  $u$  and observer  $L_\infty$  with the following formulation :

$$\left. \begin{array}{l} \dot{\hat{x}} = A\hat{x} + Bu + N(y - C\hat{x}) \\ u = -L_\infty \hat{x}, \quad L_\infty = B^T P \end{array} \right\} F_y(s) \quad (3.16)$$

This can be implemented using the implicit ARE solver in Matlab *icare*. The solution is checked by computing the  $H_\infty$  of the resulting  $G_{ec}$  which is the value of the performance parameter  $\gamma$ . To validate the final result using this method, the inbuilt loop shaping of  $H_\infty$  is used to test if the final feedback loop is optimal or can be improved. This is done by simply building an extended simple augmented plant made of mainly weights but equal to 1 as with this validation, the goal is to see if the final extended controller is able to be improved by adding more weights on the system gain.

### 3.3.3 Optimal Controller

For the optimal controller, the conditions for controllability and observability are checked through determining the controllability matrix by using *ctrb* and the observability matrix by *obsv* commands in Matlab. Then if the rank of these matrices is the same as the dynamic system then the system is observable and controllable. The check is done by subtracting the ranks of these matrices with the matrix  $A$  in the dynamic system as shown Equation 3.17.

$$\begin{array}{ll} \text{Observable} & \text{if } \rightarrow \text{rank}(A) - \text{obsv}(\text{sys}) = 0 \\ \text{Controllable} & \text{if } \rightarrow \text{rank}(A) - \text{ctrb}(\text{sys}) = 0 \end{array} \quad (3.17)$$

There *sys* is the whole dynamic system of the vehicle ( $A, B, C, D$ ). Now that the first assumption is accurate, calculate  $Q = C^T C$  and assume the disturbance intensity of the input is  $R = 1$ . Now given the assumptions for observability and controllability of the system, the quadratic problem can be solved

through  $J^*(x_0)$  by:

$$J^*(x_0) = x_0^T P x_0 \quad (3.18)$$

where  $P$  is unique positive definite solution to the Algebraic Riccati Equations **ARE** :

$$A^T P + PA + Q = PBR^{-1}B^T P \quad (3.19)$$

the optimal stabilizing feedback control to the system is :

$$\mu(x) = -R^{-1}B^T P x \quad (3.20)$$

For extensive proof of the **ARE** and its solution refer to U. Jönsson [16]. Now solve the formulated **ARE** for this problem found in Equation 3.19. The optimal feedback equation evaluated is in the following equation:

$$BR^{-1}B^T = \begin{bmatrix} 8.6614 & -0.0132 & 32.0471 & 0 \\ -0.0132 & 1.4629 & 13.9846 & 0 \\ 32.0471 & 13.9846 & 253.1967 & 0 \\ 0 & 0 & 0 & 0 \end{bmatrix} \quad (3.21)$$

Now after solving the **ARE**, the solution  $P$  is checked if positive definite by computing the eigenvalues of the  $P$  matrix. This provides an optimal feedback stabilizer in the following form.

$$\mu(x) = L_\infty = \begin{bmatrix} 0.4363 & 0.2031 & -0.2584 & -7.3802 \\ 0.7860 & -0.0211 & 0.1362 & 0.3583 \end{bmatrix} \quad (3.22)$$

Now  $L_\infty$  is set in a closed feedback loop with the open loop transfer function, which produces the new state space of the closed loop :

$$\begin{aligned} \dot{x} &= (A - BL)x + Bv \\ y &= Lx \end{aligned} \quad (3.23)$$

This helps on simplifying computation of the impulse and step responses which helps in the performance analysis of the control system and it also helps in understanding the system behavior.



# Chapter 4

## Results and Analysis

### 4.1 Modeled Aerodynamics

#### 4.1.1 Lift Coefficient Elevator Setting

The data acquired for lift coefficient  $C_L$  from both the LLM and VLM is analyzed and compared to validate and discuss the differences between the two methods. Both data sets are shown in figures 4.1 and Figure 4.2. It is important to note here that the ground effect model in Section 2.1.3 had no formulation for estimating the pitching moment but VLM had, so the main focus will be on the lift data as both models used the pitching moment data acquired from VLM. The first big difference seen in the data is that the slope of LLM is bigger, meaning the lift is predicted to be better using the LLM and the ground effect model. Second main difference is that the lift is also predicated to not differ based on elevator set compared to VLM, as the lift curves are closer to each other. This acquired data will be used to compute some performance measures and estimation to test for validity.

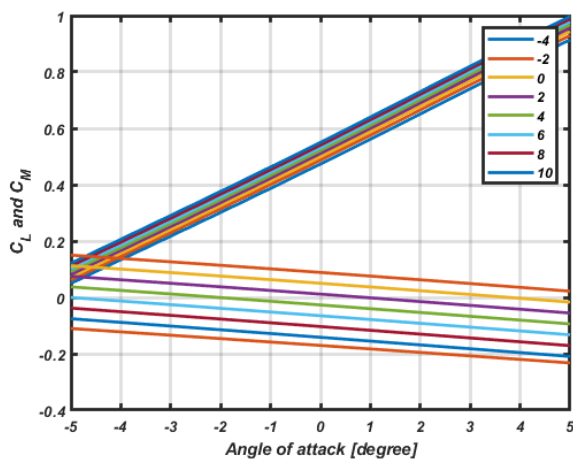


Figure 4.1: The pitching moment and lift dependent on elevator set with LLM

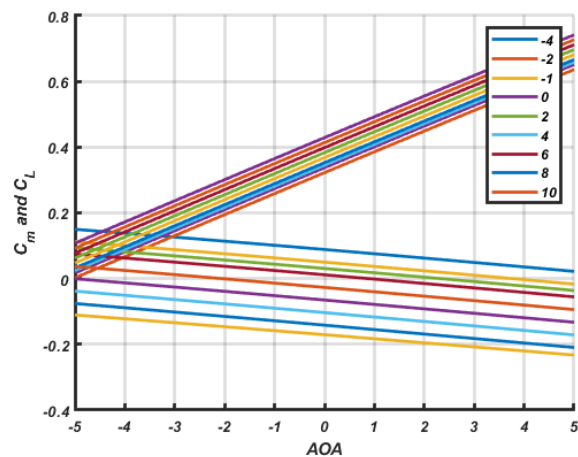


Figure 4.2: The pitching moment and lift dependent on elevator set with VLM

### 4.1.2 Lift to Drag Ratio

The lift to drag ratio is computed using both methods and the data acquired is shown in figures 4.3 and 4.4. The difference from the lift data extends to the data in the lift to drag ratio, where LLM predicts a higher ratios at higher angles of attack. It could be useful here to isolate the data from drag as the lift data differs as established already from Section 4.1.1.

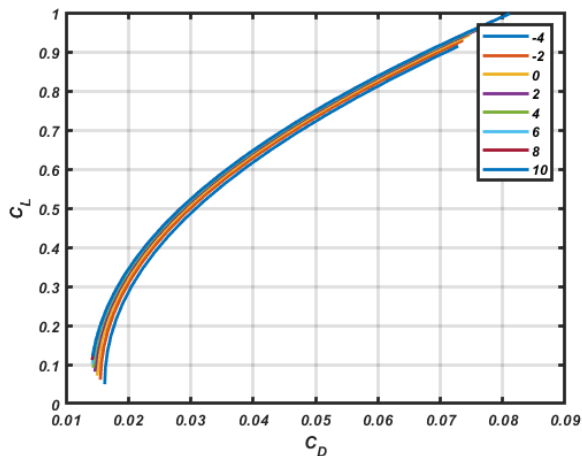


Figure 4.3: Lift to drag ration using LLM

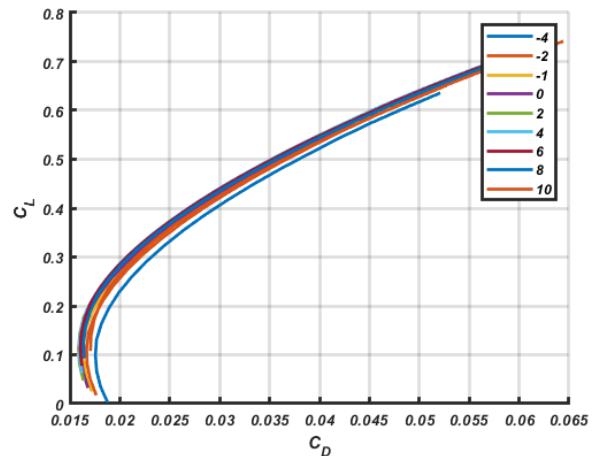


Figure 4.4: Lift to drag ratio using VLM

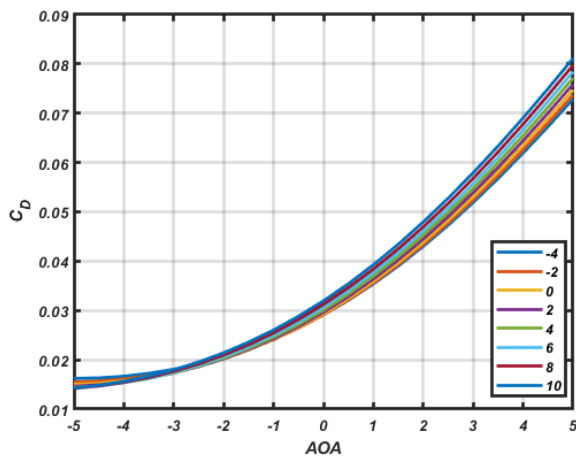


Figure 4.5: Drag coefficient dependent on angle of attack using LLM

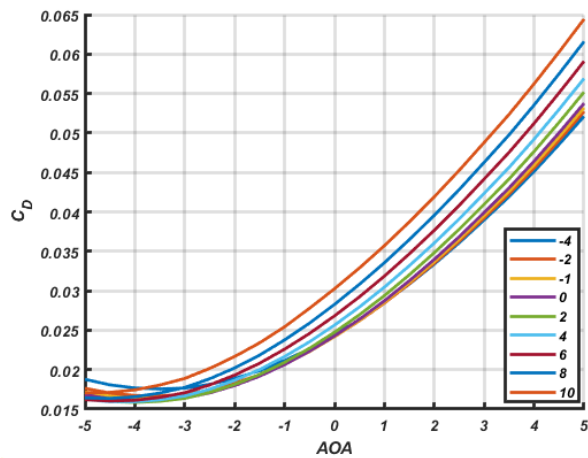


Figure 4.6: Drag coefficient dependent on angle of attack using VLM

The data for drag from both methods are plotted over the angle of attack in Figure 4.5 and Figure 4.6. The data from LLM is predicting overall a higher drag especially in angles of attack above zero.

### 4.1.3 Performance Analysis

The performance analysis is conducted on the vehicle to help in understanding instabilities and requirements needed for the control system. The analysis is mainly based on the dynamic system and the aerodynamic data from both methods.

### Trimmed vs Untrimmed:

The comparisons of the trimmed and untrimmed lift coefficient for both methods are shown in the Figure 4.7 and Figure 4.8. The difference between the trimmed and untrimmed lift for **VLM** is more clear at low and high angles of attack. The **LLM** method has less difference in lift between trimmed and untrimmed. The trimmed lift in both cases providing a higher lift coefficient of the low angles of attack which is as expected. The number of elevator angles used here is 8 from  $[-4^\circ, 10^\circ]$ .

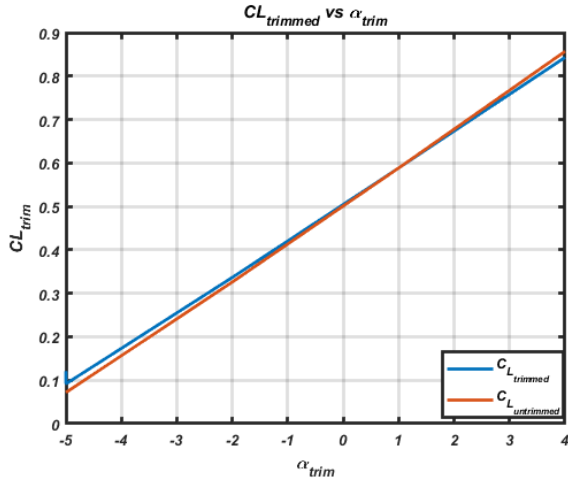


Figure 4.7: The trimmed vs untrimmed lift coefficient using **LLM**

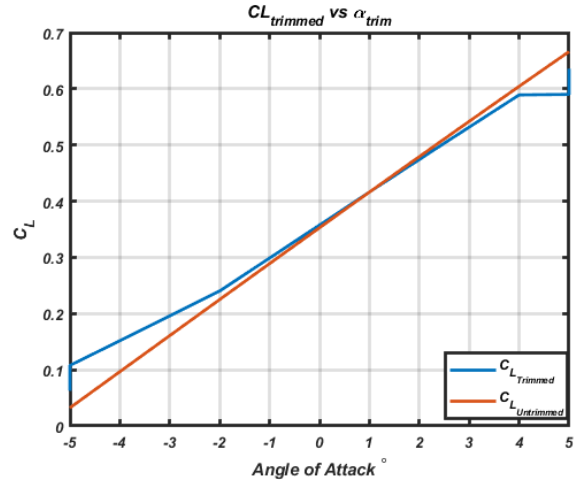


Figure 4.8: The trimmed vs untrimmed lift coefficient using **VLM**

### IGE vs OGE:

Analysis of the ground effect model is conducted to validate and check the difference in performance between the different methods. The first comparison is done on the lift coefficient **IGE** and **OGE**. Figure 4.9 and Figure 4.10 show similar behavior in the effect of ground effect on the lift of the vehicle over the different angles of attack. The increase in lift is logical and matches the theory behind the effect of ground effect as discussed in Section 3.1.1. However, unlike the pattern seen in the aerodynamics figures, it seems that the **VLM** method computes a higher influence from the ground effect on lift compared to **LLM** especially in the high angles of attack. For the **LD**, the **LLM** seems to show higher over all difference when comparing in and out of ground effect as shown in table 4.1. That shows that the integrated ground effect model in **LLM** estimates higher influence on drag than **VLM**, in the sense that the drag decrease is higher in **LLM** than **VLM**. Now it is useful to compare the ratios of **IGE** and **OGE** to see how much different is the performance of the vehicle in high altitude. The maximum lift to drag ratio is a good measure to understand the state where the vehicle is most effective. The state where the maximum lift to drag ratio occur based on both methods is shown on table 4.1.

Table 4.1: Maximum lift to drag ratio

Maximum Lift to Drag Ratio				
Method	max(L/D) IGE	max(L/D) OGE	angle of attack $\alpha$	Elevator setting $\delta_e$
<b>LLM</b>	17.7934	13.1087	-1	8
<b>VLM</b>	14.9453	13.4277	0	4

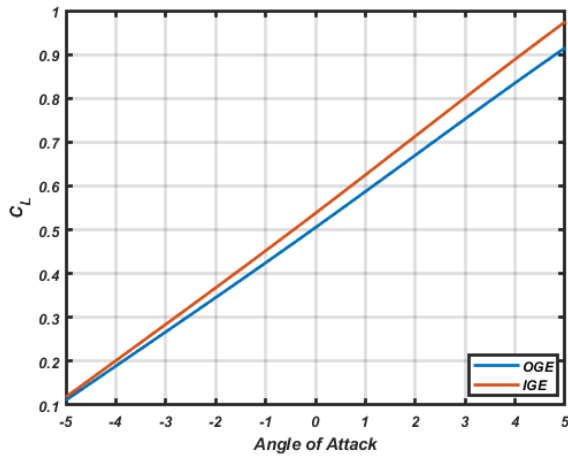


Figure 4.9: The lift data IGE and OGE with LLM

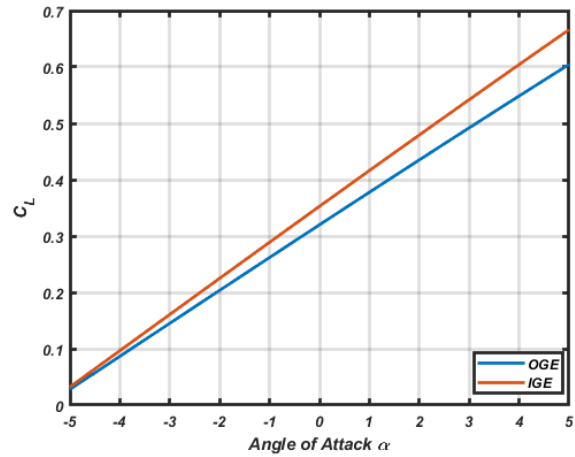


Figure 4.10: The lift data IGE and OGE with VLM

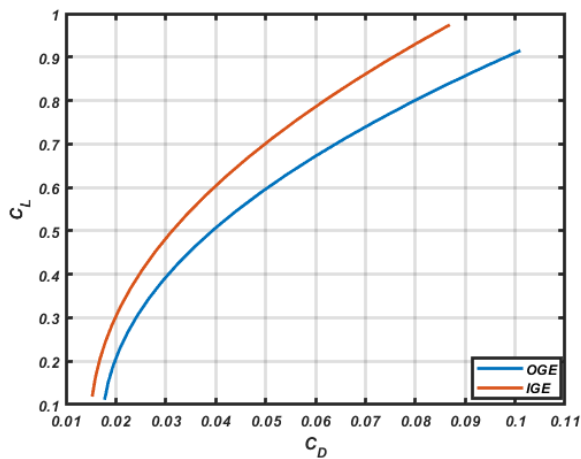


Figure 4.11: Elevator trim angle over airspeed with LLM

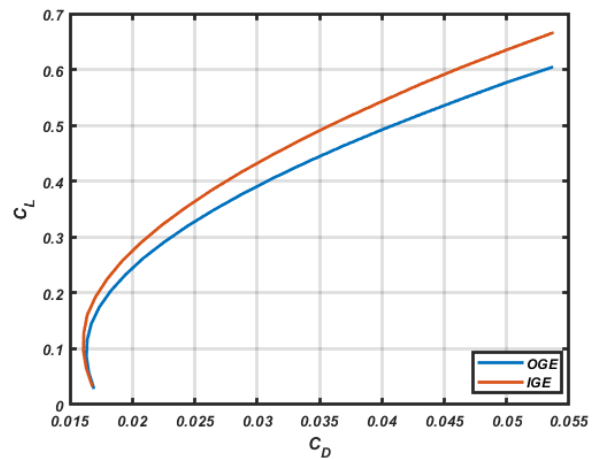


Figure 4.12: Elevator trim angle over airspeed with VLM

The LLM has a higher estimate of the maximum lift to drag ratio with harder requirement on the elevator to be set at 8 degrees, compared to VLM which has a smaller elevator angle of 4 degrees. Both have angle of attack to be between 0 and -1 degrees which is feasible since the vehicle does not have a risk to hit the ground while flying as it operates really close to the surface. When comparing IGE and OGE, the LLM have a higher influence factor from the ground effect than the VLM. These ratios of in and out of ground effect are good to analyze and check how the vehicle is effective in ground effect and how much the reduction in performance is expected in case the vehicle leaves the ground effect.

## 4.2 Modelling of Dynamics and Open Loop System

The Figure 4.13 shows the results of the solution to the trim condition where vehicle manages to stay in the same altitude and velocity for a distance of 4.5 [km] given a trim angle of  $-2,2^\circ$ . Another flight simulation is tested where the aim is to test the vehicle's ability to stabilize in case of faulty inputs. the same input from the cruise simulation are inserted but with 10-5 % increase on the elevator angles at 500 [m] distance. The results of that simulation is shown in Figure 4.14 where the vehicle stalls at 1.1 [m] altitude. The system manages to stabilize again to 0.4 [m] altitude, but after facing heavy oscillations which decrease eventually. To analyze these oscillations, the flight modes have to be investigated which is done in Section 4.2.1.

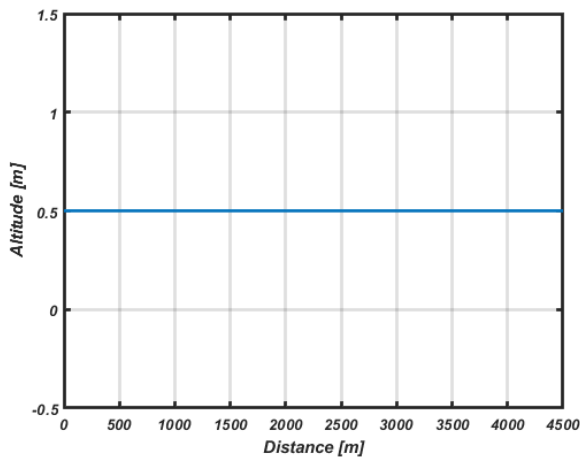


Figure 4.13: Flight simulation for the vehicle in trim condition (cruise)

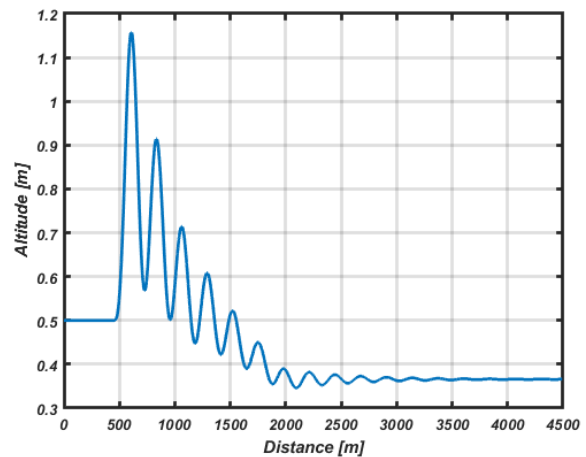


Figure 4.14: Flight simulation for the vehicle with faulty inputs

### 4.2.1 Open Loop System

These two modes are plotted on the root locus figures shown in Figure 4.16 and Figure 4.15. The main criteria for stability of these modes is that they have to stay in the left hand side of the graph, which means the eigenvalues have to stay in the negative side of the real part  $Re(z)$ . The short period mode shows stability in both position and direction, where it starts at -10 and moves to the left meaning with speed increase the vehicle is more stable in that interval. For the phugoid, the system is relatively stable as it starts at the left hand side of the imaginary plot, but it has a tendency to get closer to zero and then moves back to the left direction.

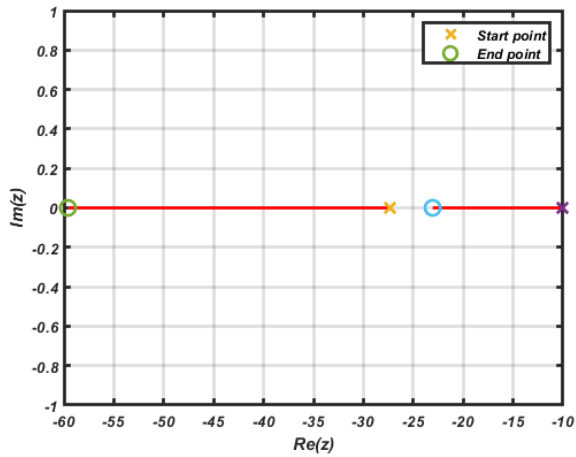


Figure 4.15: The Short period mode over airspeeds between [16-36]  $m/s$

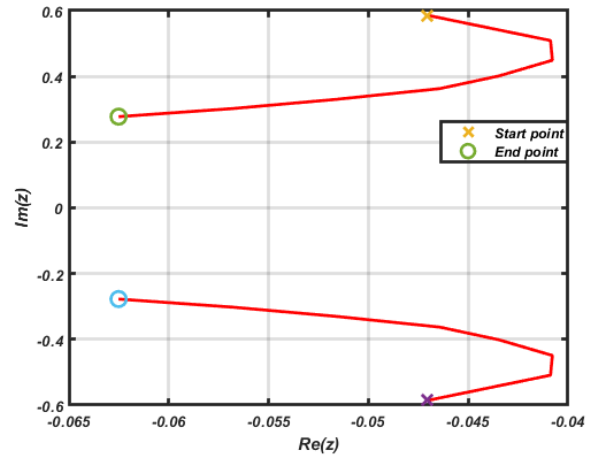


Figure 4.16: The Phugoid mode over airspeed between [16-36]  $m/s$

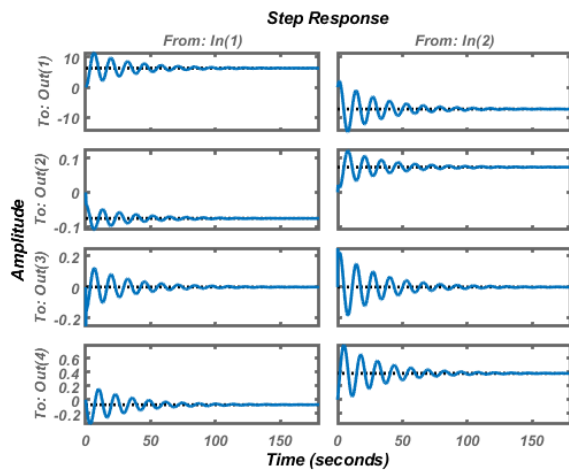


Figure 4.17: The step response of the open loop system

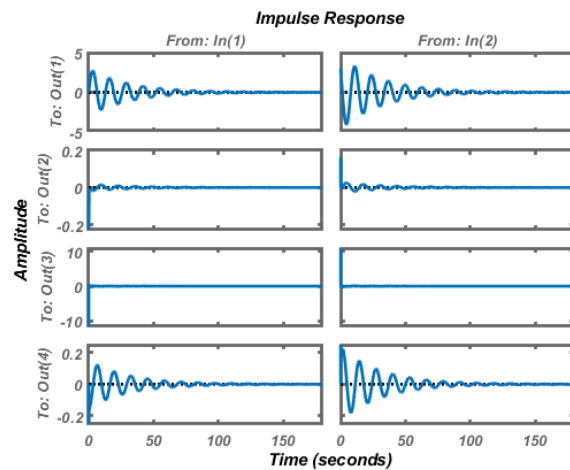


Figure 4.18: The impulse response of the open loop system

With the eigenvalues of the phugoid being this close to the right hand side, it can mean that oscillations can occur at certain speeds but no divergence. For further stability analysis of the open loop system, the computation of the step responses and impulse response is conducted and shown in figures 4.17 and 4.18. The first input in the step responses and impulse responses being the elevator angle and second input propeller power, while the outputs from the first to last are the horizontal speed, vertical speed, pitch rate and pitch angle. Both plots converge and that indicates that the system is stable. The impulse response represents the system response to disturbances and perturbation and as shown the system still manages to converge back to zero. Now given this is a **MIMO** system, this is not enough to conclude that the system is stable. As defined before the system gain has to be bounded and low to ensure no uncertainties and instabilities at specific frequencies.

As shown in Figure 4.19, the system has problematic high gain at low frequencies. That concludes that the system is unstable at low frequencies and it provides a further need for exploring and discussing a closed loop system that will be able to address this instability.

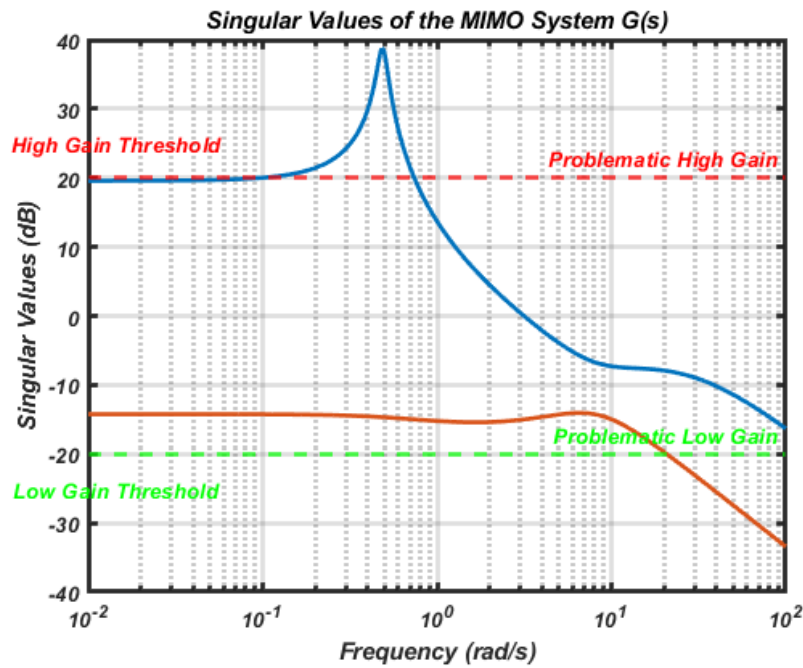


Figure 4.19: System gain for the open loop system

## 4.3 Control Systems

### 4.3.1 Pairing Problem and Decentralized Controller

The decentralized approach is tested on the whole system as discussed in Section 3.3.1. Now the pairing problem for the whole system is solved and the solution to the pairing problem for the whole system is shown table 4.2:

Table 4.2: Pairing problem solution

Relative Gain Array at $\omega_0 = 0$			Relative Gain Array at $\omega_c = 0.1$		
Output	(input 1)	Input 2	Output	(input 1)	Input 2
1	1.2692	-0.2693	1	1.4049	-0.4051
2	0.0141	-0.0117	2	0.0055	-0.0048
3	0.0000	0	3	-0.0041	0.0140
4	-0.2832	1.2810	4	-0.4064	1.3960
diagonal of RGA at $\omega_0 = 1.6259$			diagonal of RGA at $\omega_0 = 1.9613$		

The pairing problem for the whole system shows results and relations between input to output as the sum of all rows are either 1 or 0. Now the whole system amplification according to the diagonal of the RGA is 1.9613. This is still not ideal as for a stable input-output relation between all the inputs and outputs, the diagonal of RGA should be around 1. As for the other outputs, mainly 2 and 3, they have a RGA diagonal value close to 0. That indicates that the inputs have less effect on these outputs compared to the others, which are 1 and 4. In conclusion, the pairing solution is input 1 to output 1 and input 2 to output 4 based on the numbers from the RGA in both frequencies. This solution is implemented and tested through plotting the step and impulse responses of the subsystem where the connections are has the most interaction.

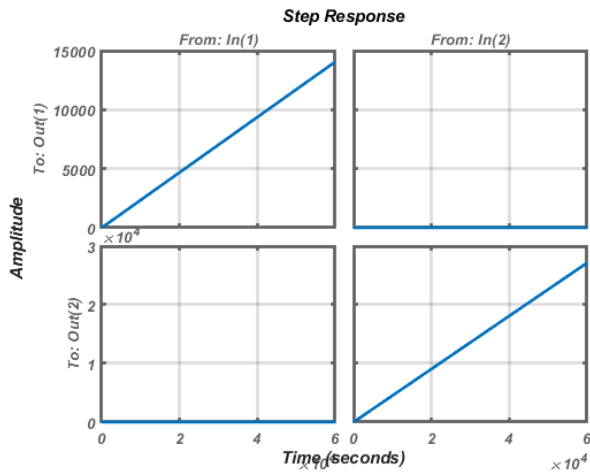


Figure 4.20: The step response of DC closed loop system

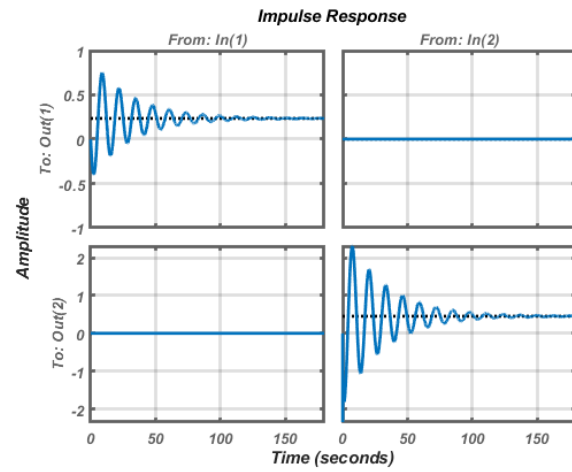


Figure 4.21: The impulse response of DC closed loop System

The step response is divergent indicating instability. This is the result of the inputs having high amplification as seen in Table 4.2 higher than 1, while having a stable impulse response. Another important distinction is that the system is decoupled, however the amplification is still present and causing instability.

### 4.3.2 H-infinite Controller

The robust controller approach is considered, with modeled uncertainty to guarantee performance given inaccuracies in the modeled dynamics. The main method focuses on augmenting the plant/dynamics system to an extended system which will take the margins to instability threshold into account. By solving the ARE implicitly, an optimized weight functions are derived for the open loop system and the performance of the systems is shown through the step response and impulse response of the system.

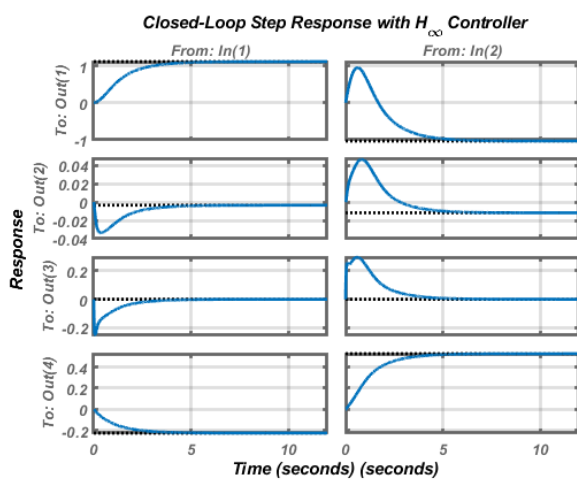


Figure 4.22: The step response of  $H_\infty$  closed loop system

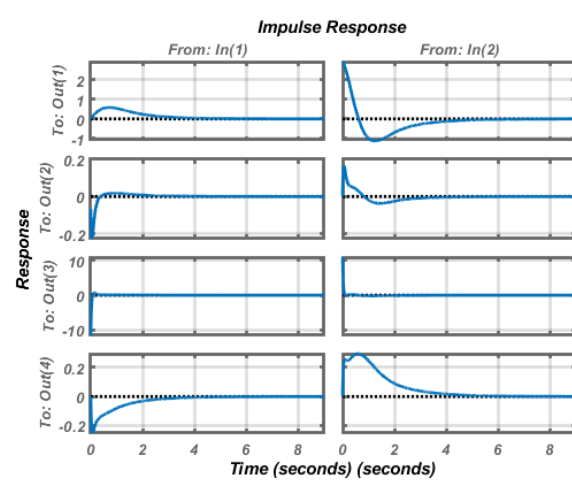


Figure 4.23: The impulse response of  $H_\infty$  closed loop System

The step response of the system converges to zero or close to zero in most outputs except (1,1) and (2,4) which matches the result from the pairing problem, as well as managing to stabilize the other outputs. That is mainly due to mathematical algorithm of the controller which attempts at minimizing the  $H_\infty$  norm over the whole system gain frequency. Since the main weight function as derived in Section 2.2.3 is the disturbance rejection, the impulse response provides a stable and fast response to disturbances where all the small disturbances and perturbations are converged back to zero. As explained in Section 2.2.1, it is not enough for a closed loop MIMO system to have poles on the left hand side, but also the directions of these poles and zeros have to be stable as well and the system gain has to be bounded. For that, the system gain of the closed loop system is plotted and shown in the following Figure 4.24.

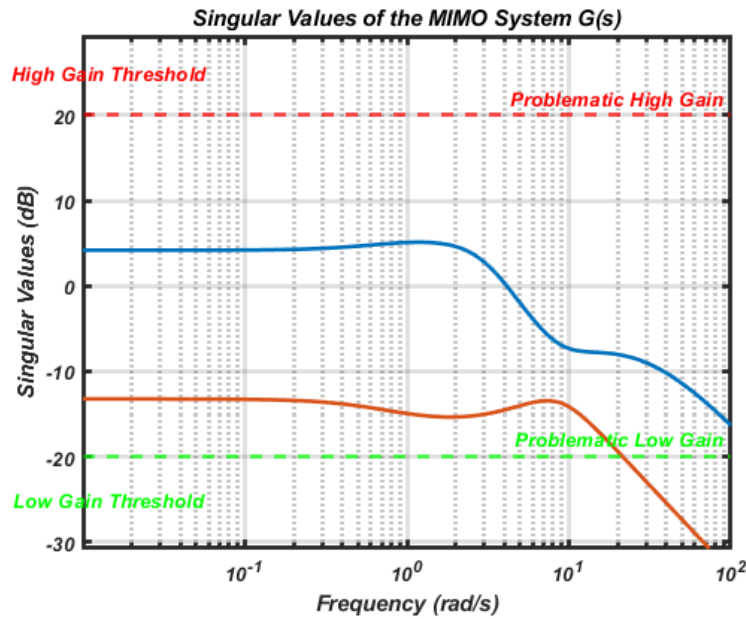


Figure 4.24: System gain for the  $H_\infty$  controller

Both the upper bound and the lower bound are in the safe threshold of the system gain except for high frequencies which represent the high input such as high speed. Since the project focuses on the vehicle in cruise state and it is assumed that it will not operate in high velocities, the vehicle is stable in the targeted speed interval. The margins for both the upper and lower bounds to reach a problematic threshold is analyzed and compared in the final comparison Section 4.3.4 as it is a robustness parameter. In summary, the system seems to be more robust in the upper bound than in the lower bound, where the threshold for problematic low gain is close to the system's lower bound presenting a higher risk of problematic low gain rather than problematic high gain. The highest system gain occurring at around frequency of 1 [rad/s] of 5.1 [dB] while the lowest occurring in the same singular value at -15.36 [dB].

### 4.3.3 Optimal Quadratic Controller

The quadratic optimal controller approach is modeled and tested. Since the battery sizing is not yet done on the vehicle, an infinite time horizon controller is considered. This is done through solving of ARE with no consideration to the performance parameter unlike the  $H_\infty$  robust controller. Instead the cost function minimizes the input and output of the system while stabilizing it, hence the name optimal feedback stabilizer. The step and impulse responses of the system are shown in Figure 4.25 and Figure 4.26 with all the input to output responses.

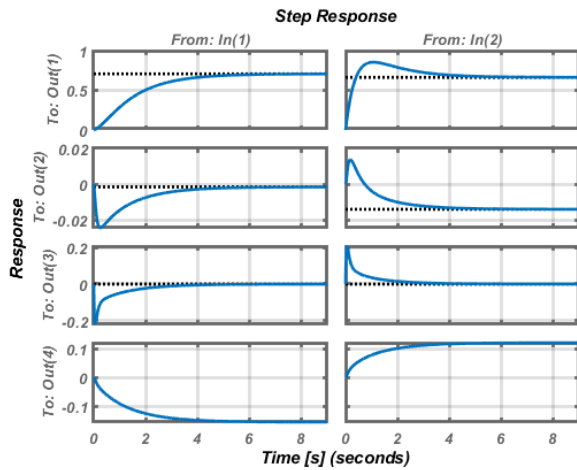


Figure 4.25: The step response of the Open Loop System

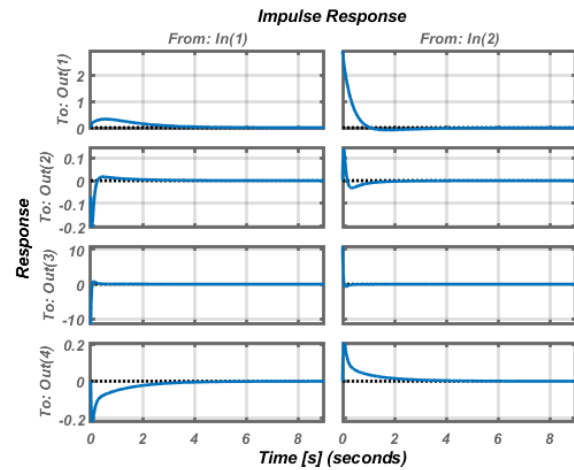


Figure 4.26: The Impulse response of the Open Loop System

The system step response and impulse response all converge to a terminal value which indicates stability. Similar to  $H_\infty$  robust controller, the behavior in the impulse response is always convergence to zero which indicates good disturbance rejection. The step response behavior is also matching with the pairing solution, where the feedback loop uses mostly outputs (1,4) which are pitch angle and horizontal speed to stabilize the system while maintaining convergence to zero on the other outputs. To quantify the performance of the system response, the parameters of rise time, settling time and overshoot will be analyzed and compared to other stable controllers. Now compute the system gain plot of for the MIMO system to check if all the direction of inputs to outputs are stable. Figure 4.27 shows the optimal control system gain with upper and lower bound. The system gain is mostly inside the non problematic threshold which means the system is stable for all frequencies except high frequencies, which is not considered in this project as mentioned before. Robust margins are higher than the ones seen before, as the margin to the high gain problematic threshold is 19.85 [dB] where the highest gain occurring at -0.15 [dB], and the margin for low threshold is 3.6 [dB] where the lowest gain occurring at -16.4 [dB].

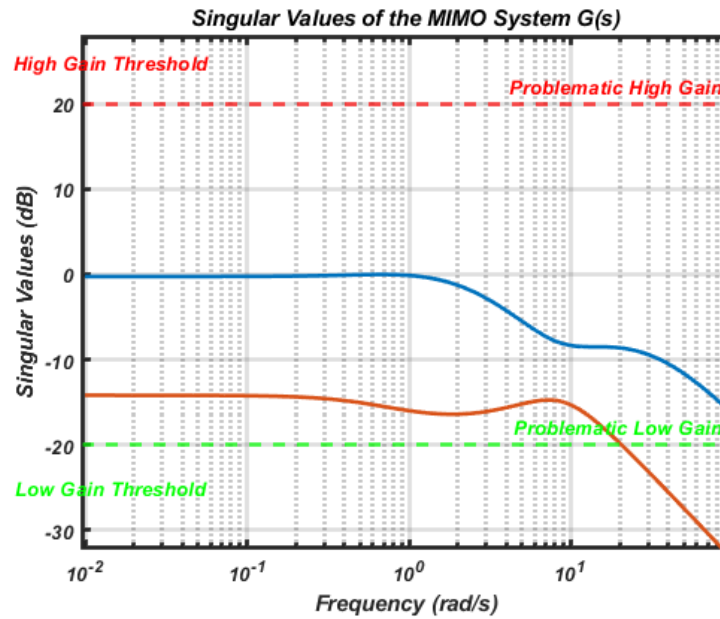


Figure 4.27: System gain for the LQ optimal controller

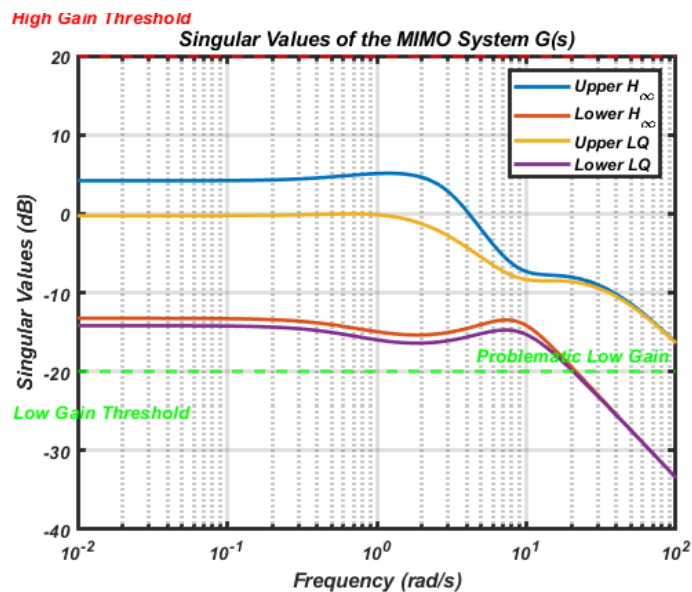
#### 4.3.4 Performance Control Analysis

In this performance analysis, the peak overshoot and peak undershoot relate to the absolute value of the overshoot rather than the percentage of error. That adjustment needed to be addressed as outputs (2,3), which are vertical speed and pitch rate angle, are converging to zero which makes taking the percentage of zero to be misleading. Rise time in the  $H_\infty$  is higher on average than  $LQ$  optimal. The average of rise time is 2.25 seconds for  $H_\infty$  while 1.75 seconds for  $LQ$ , so when it come to response time, it can be concluded that the  $LQ$  is faster at responding to inputs compared to  $H_\infty$ . For the settling time, the average time for  $H_\infty$  is 5.6 seconds while for  $LQ$  is 5.475 seconds. Both controllers are performing in a comparable manner.  $LQ$  outperforms the  $H_\infty$  in terms of initial errors where it either overshoots or undershoots with 28% before converging while marginally having faster stabilizing time. For accuracy, all the overshoot and undershoot are small and have fast rise time, except for the propeller and the horizontal speed in  $H_\infty$ , where the overshoot reaches 1.938 peak value. Overshoot occurs as well in the same connection for  $LQ$  where the overshoot is still smaller and with fast rise time. The second highest inaccuracy between the connections is the pitch rate angle, where in the  $H_\infty$ , the elevator angle causes undershoot of around 0.25 and the propeller causes an overshoot of 0.3 and a similar behavior can be observed in the  $LQ$  controller. The controllers, as mentioned before, prioritizes the pitch angle and horizontal speed as they cause most system gain and sensitivity, which is why errors appear in the pitch rate angle, however the pitch angle stays without an overshoot, which means the overshoot and undershoot in the pitch rate angle are canceling each other leading to zero errors in the pitch angle.

Table 4.3: Numerical results of the controllers performance

Controller Performance Analysis					
Controller	(Input, Output)	Rise Time [s]	Settling Time [s]	Peak Overshoot	Peak Undershoot
$H_\infty$	(1,1)	2.692	4.989	0	0
	(1,2)	2.25	7.705	0	-0.0335
	(1,3)	1.07	4.2	0	-0.25
	(1,4)	2.494	4.5099	0	0
	(2,1)	2.5799	6.2777	1.938	0
	(2,2)	2.6197	7.4556	0.05	0
	(2,3)	1.9	5.2	0.3	0
	(2,4)	2.5824	4.7219	0	0
LQ	(1,1)	3.0846	5.5146	0	0
	(1,2)	2.19	8.8715	0	-0.0224
	(1,3)	0.65	5.57	0	-0.219
	(1,4)	2.7745	4.9783	0	0
	(2,1)	0.3061	5.0338	0.189	0
	(2,2)	2.504	5.4358	0.0274	0
	(2,3)	0.458	3.6836	0.207	0
	(2,4)	2.5609	4.7495	0	0

### 4.3.5 Stability Analysis

Figure 4.28: System gain comparison between  $LQ$  and  $H_\infty$ 

Now for the margin to instability, Figure 4.28 shows the system gain of both systems. The main difference is that the  $LQ$  controller is closer to the problematic low gain threshold by a small margin of 3.6 [dB], compared to  $H_\infty$  which is 5.1 [dB] from the low threshold. In general the  $LQ$  stays in lower system gain compared to the  $H_\infty$ , which is understandable given that the optimal controller solves for the optimal inputs in the system to get an optimal performance and stability. That means the  $LQ$  will tend to choose the minimum inputs despite their distance to instability, which is the opposite of  $H_\infty$  where it will try to maximize the stability margins.  $LQ$  has the smallest lower margin compared to  $H_\infty$  which indicates that in terms of stability the controller  $H_\infty$  is more stable and robust.

Both controllers also show low problematic gain at high frequencies, indicating that the vehicle is hard to control at high speeds where the inputs on the vehicle have a risk of low gain and not being able to affect the output enough to control them. The behavior of the upper and lower bound is similar in the sense that the margin between the upper bound and the lower bound is smaller at high frequencies.



# Chapter 5

## Discussion

### 5.0.1 Generated Aerodynamics

The results from both the **VLM** and **LLM** are comparable and do not deviate too much from each other which is a good indicator to validate both methods. However, in broad terms the **LLM** was always providing higher lift compared to **VLM**. When comparing in and out of ground effect, the predictions showed that the ground effect model in **LLM** is estimating higher lift. For the **VLM**, it had the lowest change in lift to drag ratio of about 1.5, while the **LLM** estimated it to be 4.5, as stated in table 4.1. Now to conclude which estimation is more reasonable, consider the other parameters like the elevator angle for the **LLM** is at 8 and angle of attack -1, this made **VLM** results seem to be the most reasonable. This is also a safer choice overall as it is always better to assume the worst case scenario and optimize on it to get a guarantee on performance. Another important reason as to why the **LLM** seems to produce higher numbers, is because the **LLM** is not a good method to be used on aircraft with low aspect ratio. The reason being is that the lifting line theory assumes elliptical lift distribution on large span, which causes it to underestimate the effect of wingtip vortices. Wingtip vortices mainly increase the down wash of the flow distribution on wing causing additional induced drag, and less lift, which explains the overestimation of aerodynamics by **LLM**.

### 5.0.2 Implemented Control Systems

Two out of the three methods used to implement a closed loop control system provided positive stable solutions. The decentralized controller, even though was not successful in the implementation phase, still provided a good insight on the interaction of inputs and outputs, that was noticeable in the other two methods. Now with that in mind, it is not enough to conclude that the decentralized approach is completely unable to stabilize flight in ground effect. There could be alternative approaches to fixing the problems encountered in the decentralized controller, like designing a more complex decoupling which was not tested in this project. For the  $H_\infty$  and optimal controller, the performance is great with each having a certain advantage over the other. This was expected as explained in Section 2.2.1, as each one designs a control loop based on different objectives in mind. If the objective is to make a battery efficient control system that will stabilize the vehicle, then the  $LQ$  controller is the best choice. If the objective is to maximize a margins to instabilities and problematic system gain, then  $H_\infty$  is the solution.



# Chapter 6

## Conclusions and Future work

### 6.1 Conclusions

The outcomes of the project did produce positive results. The main goal is modeling of a ground effect vehicle and designing a control system that is able to stabilize it. Multiple approaches are tested and implemented to check how much they differ and which one is the most feasible one. For the aerodynamics of the vehicle, two methods were tested which are **LLM** and **VLM**. The final conclusion was that **LLM** was not appropriate for this kind of vehicles as the wing of the vehicle has a small aspect ratio and a compound wing which made it discard the induced drag on the edges of the wing. **VLM** is more efficient and produced more reasonable data that matched with design report [7] and manages to take into account the small aspect ratio of the wing. For the control systems, three methods are tested and two of them yielded stable and efficient closed loop systems. Each one of them functions according to its objective and approach. This can help in studying the trade-off between trying to be as stable as possible, which corresponds to  $H_\infty$ , or as efficient as possible, which corresponds to the optimal quadratic controller. Since this is a study conducted on a vehicle that is still in the development and testing phase, the  $H_\infty$  is the safe option here. Including the modeled uncertainty in the dynamics can guarantee some performance despite errors in the modeling and the aerodynamics of the vehicle. This also leads to the possibility of a hybrid system where the onboard computer can switch between the two algorithms based in the disturbance intensity and weather conditions. Working on the project provided a lot of insights on **MIMO** control systems for flight in general. The process of studying the vehicle performance and deriving requirements for the control system was useful. Some suggestions for other projects in this area would be to try and test new methods and not stick to the ones that are most familiar, as some methods were tested later in the process only to be a lot easier to implement than thought to be. Second suggestion would be to validate along the way in the process since this is a simulation and modeling project, so no real experiments were conducted. This meant that there had to be extra emphasis on robustness and validity of the work done. If the project was to be done again, the approach that was mentioned in the suggestions would be implemented faster to generate aerodynamic data from multiple methods to validate early on. Finally, alternative implementation methods should be tested in case the common theoretical ones are slow or computationally demanding.

## 6.2 Limitations

Some limitations are the lack of some data on the design itself. Some numbers had to be estimated manually or approximated due to some missing data. This data is mainly on the geometry of the vehicle and CFD simulations that were done on the vehicle during the design phase. This data would have simplified and improved the quality of the model over all as CFD is generally more accurate than the methods used. Mainly the extreme ground effect region, that could have opened up the possibility to see how the control system can perform in take off and check if it can stabilize it efficiently. Another limitation could be the possibility to test the control system on the miniature design of the vehicle. This could have provided a lot more validation and helped understand how reliable the results are in reality.

## 6.3 Future work

### 6.3.1 What has been left undone?

The drag estimation on the fuselage is to be taken into account when generating the aerodynamics of the data. This will lead to a decrease in the lift to drag ratio of the vehicle, which will affect the performance of the control system. However, by having reliable margins like in the  $H_\infty$  controller, the control system should be able to handle some unexpected bad performance by the vehicle, but having this data can help provide more accurate performance by the control system.

### 6.3.2 Next obvious things to be done

The design of the vehicle has a third input to help control it longitudinally and that is the propeller angle. This is an important feature in the design which can add extra complexity but also efficiency for stabilizing the vehicle in ground effect. The main function of that input is mainly to help in the take-off phase which is not something considered in the project. Simulating the vehicle in CFD and including the thrust angle as an input would be the next task to be done on the project. This would help in designing a control system for the take off and then the vehicle will be fully autonomous longitudinally.

## 6.4 Reflections

The project is meant to contribute for a ground effect vehicle design in its early stages. This vehicle is going to be analyzed and studied as a more efficient and sustainable alternative solution to modern transportation. Sustainability is becoming an important factor in modern engineering projects as the effects of pollution and climate change are becoming ever more apparent on the planet. The efficiency and speed of these vehicles makes them sustainable compared to standard aviation and faster than modern seafaring. It is a solution that provides the best aspects of two different modes of transport, which could be big part of future transportation.

# References

- [1] Bert Lenaerts, Florian Allroggen, and Robert Malina. “The economic impact of aviation: A review on the role of market access”. In: *Journal of Air Transport Management* 91 (2021), p. 102000. ISSN: 0969-6997. DOI: <https://doi.org/10.1016/j.jairtraman.2020.102000>. URL: <https://www.sciencedirect.com/science/article/pii/S0969699720305822>.
- [2] Hannah Ritchie. “What share of global CO2 emissions come from aviation?” In: *Our World in Data* (2024). <https://ourworldindata.org/global-aviation-emissions>.
- [3] Stefan Ellerbeck. “The aviation sector wants to reach net zero by 2050. How will it do it?” In: *World Economic Forum* (Dec. 2022). <https://www.weforum.org/agenda/2022/12/aviation-net-zero-emissions/>.
- [4] Raymond Jaworowski. “Heart Aerospace Unveils Full-Scale Demonstrator for ES-30 Program”. In: *Flight Plan* (Sept. 2024). <https://flightplan.forecastinternational.com/2024/09/18/heart-aerospace-unveils-full-scale-demonstrator-for-es-30-program/>.
- [5] Casey Crownhart. “This is what’s keeping electric planes from taking off”. In: *MIT technology Review* (Aug. 2022). <https://flightplan.forecastinternational.com/2024/09/18/heart-aerospace-unveils-full-scale-demonstrator-for-es-30-program/>.
- [6] Snorri Gudmundesson. *General Aviation Aircraft Design: Applied Methods and Procedures*. Elsevier Inc, 2014.
- [7] Alfonso Penela et al. “Wing-in-ground effect”. In: *KTH* (2020).
- [8] Mark Drela. *Flight Vehicle Aerodynamics*. International series of monographs on physics. The MIT Press, 2014.
- [9] Bernard Etkin and Lloyd Duff Reid. *Dynamics of Flight*. Third. John Wiley & Sons Inc, 1996.
- [10] W.F Philips and D.F Hunsaker. “Lifting-Line Predictions for Induced Drag and Lift in Ground Effect”. In: *Journal of Aircraft* 50 (2013).
- [11] John J. Bertin and Micheal L. Smith. *Aerodynamics for Engineers*. 3rd ed. Prentice Hall Inc, 1998. Chap. 7.
- [12] Xin Shen, Zhaohui Du, and Xiao cheng Zhu. “Load control and unsteady aerodynamics for floating wind turbines”. In: *Proceedings of the Institution of Mechanical Engineers Part A Journal of Power and Energy* 235 (Feb. 2021). DOI: [10.1177/0957650921993255](https://doi.org/10.1177/0957650921993255).
- [13] Torkel Glad and Lennart Ljung. *Control Theory: Multivariable and nonlinear methods*. 11 New Fetter Lane, London: Taylor & Francis, 2000.
- [14] Achu K R and Subhasish Mahapatra. “Frequency Domain Specifications Based Robust Decentralized PI/PID Control Algorithm for Benchmark Variable-Area Coupled Tank Systems”. In: *Sensors* 22 (Nov. 2022), p. 9165. DOI: [10.3390/s22239165](https://doi.org/10.3390/s22239165).

- [15] Elling Jacobsen. *MIMO Robust Stability Hinfinity-optimal Controller Design*. May 2023.
- [16] Ulf Jönsson, Claes Trygger, and Petter Ögren. *Optimal Control: Lecture Notes*. Royal Institute of Technology, 2010.
- [17] Dennis G. Zill and Warren S. Wright. *Differential Equations with Boundary-Value Problems*. Cengage Learning, 2012. Chap. 2.
- [18] Kirill V. Rozhdestvensky. *Aerodynamics of a lifting System in Extreme Ground Effect*. Springer-Verlag Berlin Heidelberg, 1945. Chap. 7.
- [19] Brain L. Stevens, Frank L. Lewis, and Eric N. Johnson. *Aircraft Control and Simulations*. 3rd ed. John Wiley & Sons, Inc, 2015. Chap. 3.

TRITA-SCI-GRU 2024:473